La investigación reportada en esta tesis es parte de los programas de investigación del CICESE (Centro de Investigación Científica y de Educación Superior de Ensenada, Baja California).

La investigación fue financiada por el SECIHTI (Secretaría de Ciencia, Humanidades, Tecnología e Innovación).

Centro de Investigación Científica y de Educación Superior de Ensenada, Baja California

Master of Science in Marine Ecology

Reconstructing temporal variability in carbon sources from the Southern California Bight and the influence of environmental change using essential amino acids $\delta^{13}C$ values from a small cetacean

A dissertation
submitted in partial satisfaction of the requirements for the degree
Master in Science

By:

Cinthia Lizeth Velazquez Matus

Ensenada, Baja California, México
2025

A Dissertation Presented by

Cinthia Lizeth Velazquez Matus

And approved by the following Committee

Dra. Rocio Iliana Ruiz-Cooley
Director of thesis

Dra. Paulina Cetina Heredia

Dr. Juan Carlos Herguera García

Dr. Rafael Andrés Cabral Tena
Coordinator of Postgraduate in Marine Ecology

Dra. Ana Denise Re Araujo
Director of Studies of Postgraduate

Resumen de la tesis que presenta **Cinthia Lizeth Velazquez Matus** como requisito parcial para la obtención del grado de Maestra en Ciencias en Ecología Marina.

Reconstruyendo la variabilidad temporal de las fuentes de carbono de la Ensenada del Sur de California y la influencia del cambio ambiental utilizando valores de $\delta^{13}C$ de aminoácidos esenciales de un pequeño cetáceo.

Resumen aprobado por:

Dra. Rocio Iliana Ruiz-Cooley
Directora de tesis

Se evaluó la variabilidad interanual de $\delta^{13}C$ en aminoácidos esenciales (AAEs) de delfines comunes (*Delphinus delphis*) capturados incidentalmente en pesquerías de redes agalleras en la Ensenada del Sur de California, E.U.A, entre 1990 y 2008, en relación con la temperatura del agua, la productividad primaria (Chl-*a* como proxy), el carbono inorgánico disuelto (CID) y el índice de surgencia costera (CUTI). Se analizaron 178 muestras de piel (tejido completo) y de estas, 30 muestras se usaron para el análisis de $\delta^{13}C$ en AAEs. Los valores de $\delta^{13}C$ en tejido completo no mostraron diferencias significativas entre años. En contraste, los valores de $\delta^{13}C$ de AAEs revelaron patrones temporales distintos: lIsina, metionina y fenilalanina presentaron las mayores fluctuaciones (6–10‰), mostrando una tendencia hacia valores más ligeros, mientras que Leu mostró un enriquecimiento progresivo. Valina, Isoleucina y Treonina no evidenciaron cambios consistentes. En promedio, los valores de $\delta^{13}C_{AAEs}$ disminuyeron 3.5‰ entre 2000 y 2008, una magnitud muy superior a la atribuible al efecto Suess (~0.2‰ por década), lo que sugiere que factores oceanográficos, más allá del forzamiento atmosférico, moldearon la señal isotópica. Los modelos aditivos generalizados (GAMs) identificaron a la temperatura, el CID y la Chl-*a* como los predictores más importantes, explicando hasta el 76% de la variabilidad isotópica. Estos resultados demuestran que los delfines comunes, al ser muestreadores biológicos del ecosistema, integran a través de su dieta la señal isotópica de los productores primarios. Estos valores de $\delta^{13}C_{AAEs}$ reflejan la variabilidad temporal del ciclo del carbono marino. A diferencia de enfoques tradicionales, como el $\delta^{13}C$ de materia orgánica particulada, que puede verse influenciado por contribuciones bacterianas, o el $\delta^{15}N$ del zooplancton, que refleja efectos tróficos, el uso de $\delta^{13}C_{AAEs}$ en depredadores tope proporciona una herramienta novedosa y más precisa para rastrear los cambios en la fijación de carbono por los productores primarios que sostienen la red alimentaria de la que se alimenta el depredador. Esta tesis resalta el potencial del análisis isotópico de aminoácidos esenciales en piel de delfín, centinelas del ecosistema que habitan, para comprender la dinámica del ciclo de carbono en respuesta a una alta variabilidad ambiental.

Palabras clave: fijación de carbono, depredador, centinela, variabilidad ambiental, isótopos.

Abstract of the thesis presented **by Cinthia Lizeth Velazquez Matus** as a partial requirement to obtain the Master of Science degree in Marine Ecology.

Reconstructing temporal variability in carbon sources from the Southern California Bight and the influence of environmental change using essential amino acids $\delta^{13}C$ values from a small cetacean

Abstract approved by:

Dra. Rocio Iliana Ruiz-Cooley
Thesis Director

Interannual variability of $\delta^{13}C$ in essential amino acids (EAAs) of common dolphins (*Delphinus delphis*) incidentally caught in gillnet fisheries in the Southern California Bight, U. S., was evaluated between 1990 and 2008, in relation to seawater temperature, primary productivity (Chl-*a* as a proxy), dissolved inorganic carbon (DIC), and the coastal upwelling transport index (CUTI). A total of 178 skin samples (bulk tissue) were analyzed, with a subset of 30 used for EAAs analysis. Bulk $\delta^{13}C$ values showed no significant differences across years. In contrast, EAAs values revealed distinct temporal patterns: Lysine, methionine, and phenylalanine displayed the greatest fluctuations (6–10‰), trending toward lighter values, while leucine showed progressive enrichment. Valine, Isoleucine, and Threonine exhibited no consistent changes. On average, $\delta^{13}C_{EAAs}$ declined by 3.5‰ between 2000 and 2008, a magnitude far exceeding the Suess effect (~0.2‰ per decade), suggesting that oceanographic drivers beyond atmospheric forcing shaped the isotopic signal. Generalized additive models (GAMs) identified temperature, DIC, and Chl-*a* as the most important predictors, explaining up to 76% of isotopic variability. These results demonstrate that common dolphins are biological samplers of the ecosystem, integrating through their diet the isotopic signal of primary producers. $\delta^{13}C_{EAAs}$ values thus reflect the marine carbon cycle. Unlike traditional approaches, such as $\delta^{13}C$ of particulate organic matter, which may be influenced by bacterial contributions, or $\delta^{15}N$ of zooplankton, which reflects trophic-level effects, the $\delta^{13}C_{EAAs}$ in top predators offer a novel and more precise tool to trace changes in carbon fixation by the primary producers that support the food web where the predators forage. This thesis highlights the potential of isotopic analysis of essential amino acids in dolphin skin, sentinels of the ecosystem they inhabit, to understand the dynamics of the carbon cycle in response to high environmental variability.

Keywords: carbon fixation, predator, sentinel, environmental variability, isotopes.

Dedication

A mis padres por enseñarme a volar y el valor para soñar en grande. Su amor y confianza en mí han sido mi fuerza. Me acompañan en dondequiera que esté, en cada pensamiento y en cada atardecer.

A ustedes, mi gratitud eterna.

Acknowledgements

I thank Centro de Investigation Científica y de Educación Superior de Ensenada, Baja California (CICESE) and Secretaría de Ciencia, Humanidades, Tecnología e Innovación (SECIHTI) for providing financial support, as well as the facilities and resources that enabled me to successfully carry out my research project.

I thank the National Oceanic and Atmospheric Administration (NOAA) and I thank the many CA Gillnet Fishery Observers who collected the samples, and personnel in NOAA's West Coast Region and Southwest Fisheries Science Center (SWFSC), Marine Mammal and Turtle Division, who administer the fishery program. I thank Lisa T. Ballance for supporting the processing of samples for isotopic analysis. I thank CalCOFI for providing access to its databases, as the wealth of information they contain is invaluable for advancing scientific research.

I would like to thank the Ecosystems & Food Web Lab for allowing me to be part of this wonderful group of people, where I learned so much from each member while also building friendships and work environments that encouraged me to grow both as a student and as a person. I am especially grateful to my advisor, Dr. R. Iliana Ruiz-Cooley, leader of this research group, for guiding me throughout my entire research process and sharing all her knowledge. I particularly appreciate her willingness to always answer my questions and review my writings, as well as her constant motivation to keep me moving forward and her encouragement to cultivate my creativity.

To the members of my committee, thank you for dedicating your time and for the valuable comments and observations you shared. Your guidance motivated me throughout this process.

I am also deeply grateful to all my teachers for sharing their knowledge and experiences, and for inspiring me. Each of your lessons has now become a part of me.

***

A mi familia, mis abuelos, mis hermanas y mi sobrino, por ser mi refugio y mi fuerza silenciosa. Gracias por su apoyo incondicional, por creer en mí y animarme en cada paso mientras sigo mi pasión. Los llevo siempre en mi corazón, como un faro que ilumina mi camino y acompaña cada sueño que persigo.

Marifer B., por siempre estar ahí, en los mejores y más difíciles momentos, por ser una gran compañera de desvelos y tazas de café, gracias por todos los atardeceres y por motivarme. Este camino no habría sido lo mismo sin ti.

Carmen M., gracias por tu ejemplo y por mostrarme de lo que somos capaces.

Fatima V., gracias por todo tu apoyo, a pesar de la distancia siempre te sentí muy cerca de mí. Por siempre extender tu mano hacia mí y no dejarme sola jamás, te quiero hermana.

Adán A., por todas las clases de bioestadística, por ayudarme a entender de una manera sencilla y perdurable, por toda tu paciencia y sobre todo por tus enseñanzas estadísticamente significativas.

Carlos V., gracias por tu amistad de ya casi toda una vida. Un recuerdo constante de que las amistades verdaderas, perduran en el tiempo.

Fernanda B., gracias por siempre confiar en mí y recordarme de lo que soy capaz, por trasmitirme tu amor y apoyo a pesar de la lejanía. Eres mi inspiración y mi lugar seguro.

Gerardo S., tu amor y compañía fueron mi soporte durante este proceso. Gracias por las sonrisas que iluminaron mis días, por cada abrazo que me sostuvo y por cada palabra que me alentó a no rendirme. Te estaré por siempre agradecida.

Gracias, Ensenada, por recibirme y llenar mi corazón con tus paisajes hermosos que brindan tanta paz a mi alma. Aquí he creado recuerdos que perdurarán por siempre.

Y gracias al mar, inmenso y eterno, por ser mi fuente inagotable de inspiración y pasión.

Table of contents

Page

List of figures

Page

List of tables

Page

Chapter 1. Introduction

The California Current System (CCS) is a highly productive ecosystem that represents one of the major coastal upwelling zones. As such, it supports rich biodiversity and sustains one of the largest fisheries in the world (Checkley and Barth, 2009). The CCS encompasses the California Current (0-300 m deep), which transports cold, northern water masses equatorward along the continental slope of the west coast of North America, ultimately feeding into the North Equatorial Current (Lynn & Simpson, 1987). It is also influenced by relatively warmer poleward-flowing subsurface waters from the California Undercurrent, Davidson Current, and Southern California Countercurrent (Figure 9; Hickey, 1979). The interplay of these major currents, along with the interannual variation in the intensity of coastal upwelling, influences primary biomass and food web dynamics (Carr, 2002).

To understand the fluctuations in the physical and biochemical environment and their effect on marine communities, the California Cooperative Oceanic Fisheries Investigations (CalCOFI) program was established in 1949 to monitor the Southern California Bight (SCB), making it one of the most studied marine regions in the world (McClatchie, 2014). The oceanographic characteristics of the SCB are highly dynamic due to the effect of large-scale climatic events such as *El Niño*-Southern Oscillation (ENSO) (McGowan et al., 1998). Notably, extreme climatic events with positive temperature anomalies such as *El Niño* event (the warm phase of the ENSO), and recent marine heatwaves (MHWs) (McGowan, 1998; Oliver et al., 2018), have had devastating impacts on marine communities, leading to biological mass mortality, increase incidence of harmful algal blooms and shifts in species distribution across marine ecosystems (Bond et al., 2015; Cavole et al., 2016; McCabe et al., 2016; Di Lorenzo and Mantua, 2016; Smale et al., 2019; Smith et al., 2022). *El Niño* events and MHWs are expected to increase in frequency and duration (Frölicher et al., 2018; Oliver et al., 2021), in turn, such trends could reduce primary productivity, impact the foraging success of many species (Di Lorenzo et al., 2005; Cai et al., 2014), and consequently drive major changes in the food web structure (Ruiz-Cooley et al., 2017, 2024). Quantifying changes in primary production and carbon fixation through photosynthesis in response to environmental variation is essential for understanding ecosystem productivity and the state of food webs (Boyce et al., 2010; Cavole et al., 2016).

In the SCB, phytoplankton abundance and species composition vary seasonally, inter-annually, and on interdecadal timescales showing remarkable shifts between anomalously warm and cold climatic

events (Kim et al., 2009). Separating the environmental impact of ENSO from those of other interannual environmental variations is challenging, as the intensity and timing of *El Niño* and *La Niña* (cold phase) vary over time within the highly complex CCS (Ware, 1995). Anomalous high sea surface temperatures (SST) and a reduction in the intensity of coastal upwelling induce a deeper thermocline, lower nutrient availability at the surface, which results in lower phytoplankton abundance (Kudela & Chavez, 2000). During these anomalous warm conditions, picophytoplankton (cells of < 2 µm in diameter) tend to dominate the phytoplankton community. In contrast, microphytoplankton (cells of > 20 µm in diameter; mainly diatoms and large dinoflagellates) favor higher biomass during cold conditions, i.e. *La Niña*, due to increased nutrient availability driven by intense upwelling (Masotti et al., 2011; Marañon et al., 2012). Spring to early summer is the most productive season of the year as pulsed upwelling and increasing daylight hours trigger phytoplankton blooms that sustain coastal food webs (Checkley & Barth, 2009). Hence, temporal variability in the phytoplankton community and primary production has critical implications for food web length, energy transfer efficiency, carbon sequestration, and ecosystem resiliency (Schlenger et al., 2018). However, quantifying these changes over time, particularly the fraction of organic carbon that enters and moves through pelagic food webs, remains challenging.

In marine ecosystems, stable isotope analysis (SIA) of carbon ($\delta^{13}C$) is widely used to investigate carbon cycling processes. Across ecosystems, the $\delta^{13}C$ values provide information about the origin of primary sources and transformations of inorganic and organic carbon (Peterson & Fry, 1987). The $\delta^{13}C$ of particulate organic carbon (POC) from the euphotic zone is heavily influenced by phytoplankton since dissolved CO_2 is used during photosynthesis (Jo et al., 2021). In the surface ocean, the $\delta^{13}C$ values of dissolved inorganic carbon (DIC) range from 0.5‰ to 2.5‰ (Gruber et al., 1999) while those of particulate organic carbon (POC) range from -19 to -26‰ across a broad latitudinal gradient (Goericke & Fry, 1994). In deeper waters $\delta^{13}C$ DIC values become lighter due to the remineralization of isotopically light POC that sinks from the surface (Tagliabue & Bopp, 2008). Regarding $\delta^{13}C$ POC values are on average 1.4‰ lower than those observed in the upper euphotic zone (Close & Henderson, 2020).

These variations are the result of isotopic fractionation driven by external inputs and outputs, and biological activity (Tagliabue & Bopp, 2008). During photosynthesis, isotopic fractionation (ε_p) varies from 5‰ to 27‰, which depends on the concentration of aqueous CO_2, intracellular CO_2 levels, cell wall permeability, cellular carbon uptake, and metabolic pathways (Raven & Johnston, 1991; Laws et

al., 1995, 1997; Rau et al., 1996; Popp et al., 1998, 1999). Spatial and temporal variation in POC $\delta^{13}C$ values is associated with shifts in temperature, light, CO_2 concentrations, nutrient availability, growth rates, and community composition (Descolas-Gros & Fontugne, 1990; Rau et al., 1991; Sachs et al., 1999; Burkhardt et al., 1999). The resultant POC $\delta^{13}C$ values reflect the environmental conditions under which carbon fixation occurred during photosynthesis (Farquhar et al., 1982).

Humans have altered the global carbon cycle, and the isotope ratios of atmospheric CO_2 (Gruber et al., 1999). The increase in CO_2 emissions, since the Industrial Revolution, mainly due to the burning of fossil fuels and deforestation (Keeling et al., 1989), has caused a global decrease in $\delta^{13}C$ values in the atmosphere and consequently in the ocean, a phenomenon known as the Suess effect (Gruber et al., 2002). In 1860, the decline in $\delta^{13}C$ DIC was about 0.07‰ per decade, but from 1970 it accelerated to 0.18‰ per decade, or about 2.6 times faster (Sonnerup et al., 1999). Overall, the oceanic Suess effect represents approximately 65% of the observed variation in atmospheric CO_2 $\delta^{13}C$ (0.27‰ per decade; Tagliabue & Bopp, 2008).

These anthropogenic CO_2 emissions have caused ocean acidification and changes in the ocean's general circulation, resulting in a severe negative impact on marine ecosystems (Hoegh-Guldberg et al., 2007; Breitburg et al., 2018). Acidification processes drive coral bleaching and biodiversity loss, which directly and indirectly affect fish populations, animal migration patterns, reproductive success, global fisheries, and food security (Caldeira & Wickett, 2003; Hoegh-Guldberg & Bruno, 2010). In this context, the biological pump is of great importance to sequester carbon from the atmosphere to the deep ocean (Ducklow et al., 2001; Volk & Hoffert, 2013). Phytoplankton assimilate CO_2 through photosynthesis to create organic matter. When phytoplankton cells die, some of their carbon-rich cell fragments sink to deeper ocean layers as marine snow, effectively removing CO_2 from the atmosphere. As this particulate organic matter (POM) descends, it is further utilized by heterotrophs in the water column before accumulating in the sediments, where carbon can be stored for long periods (Longhurst & Harrison, 1989). The proportion of phytoplankton biomass that enters marine food webs through animal consumption and is transferred to top predators can reveal how carbon sources have varied over time and help to identify the environmental factors driving these changes.

The phytoplankton community represents the base of pelagic food webs, and their $\delta^{13}C$ values are considered baseline values, as they reflect the fixed carbon sources within a specific geographic area, time, and environmental conditions (Rau, 1991; Goericke & Fry, 1994). These $\delta^{13}C$ baseline values are

integrated by primary consumers through their diet and are subsequently transferred through the food web. In a local community, the $\delta^{13}C$ values in bulk tissue of consumers typically increase by 0.5 to 1‰ with each trophic level (DeNiro & Epstein, 1978). Therefore, $\delta^{13}C$ values in bulk of animal tissues (including those of top predators) integrate and reflect information from the primary producers supporting the food web and their diet over a period that depends on the specific tissue analyzed (Tieszen et al., 1983). These values can reveal the carbon sources and pathways of energy and elemental flow through marine food webs (Hobson et al., 1994). In cetaceans, the skin is the most readily accessible tissue for sampling free-ranging individuals, and its turnover rate is on average 70 days (Hicks et al., 1985). The $\delta^{13}C$ and $\delta^{15}N$ in the odontocete skin reflect information for a period of three months to potentially six months prior to sampling (Hicks et al., 1985; Browning et al., 2014; Ruiz-Cooley et al., 2014). Nevertheless, $\delta^{13}C$ in bulk tissues (bulk SIA) often lacks source specificity due to variable isotope discrimination and shifts in primary producers across space and time (McClelland & Montoya, 2002, Post, 2002). This limitation can hinder the interpretation of results, especially when baseline variability has not been characterized.

To address these limitations, $\delta^{13}C$ of individual amino acids (AAs) measured in animal tissues can effectively separate baseline variability from dietary effects (McClelland & Montoya, 2002; Popp et al., 2007; Chikaraishi et al., 2009). The $\delta^{13}C$ of AAs are grouped into essential AAs (EAAs, which cannot be synthesized by animals and must be obtained from the diet) and nonessential (NEAAs; that can be synthesized by animals) (McClelland & Montoya, 2002; Schmidt et al., 2003; Larsen et al., 2013). The $\delta^{13}C$ values for EAAs reflect primary producers´ values, which can be detected in consumers from any trophic position (Larsen et al., 2013; Ohkouchi et al., 2015), including marine top predators (Newsome et al., 2010; Larsen et al., 2013; Ruiz-Cooley et al., 2014). As a result, the carbon backbones of EAAs serve as powerful tracers of primary producers, as $\delta^{13}C$ EAAs values remain largely conserved as they are transferred from producers to apex predators (Larsen et al., 2009; Ohkouchi et al., 2015). However, not all EAAs have the same $\delta^{13}C$ values, because AAs are synthesized through different metabolic pathways (such as glycolysis, the tricarboxylic acid (TCA) cycle, or the pentose phosphate pathway), which build their carbon skeletons (Brett et al., 2017). Additionally, phylogenetic differences among primary producers exist, which include variations in how they fix inorganic carbon (CO_2 or HCO_3^-), and different AAs concentrations depending on the needs of specific phytoplanktonic communities (Kolmakova & Kolmakov, 2019), which influence their $\delta^{13}C$ values. Consequently, variations in AAs isotopic values reflect both the biosynthetic pathways of individual AAs and the environmental conditions regulating photosynthesis.

Because consumers integrate these $\delta^{13}C$ baseline values into their tissues through diet, predators serve as natural biological samplers of their environment (Ruiz-Cooley et al., 2014). They can reflect variability in both baseline values and trophic dynamics across space and time (Ruiz-Cooley et al., 2017). In the offshore CCS, sperm whale skin samples revealed a 3‰ decline in essential amino acid $\delta^{13}C$ values from 1993 to 2005, pointing to rapid changes in the phytoplankton assimilation (Ruiz-Cooley et al., 2014). While the Suess effect accounts for part of this decline (~0.2‰ per decade since 1960, Francey et al., 1999), additional factors, such as shifts in the phytoplankton composition or altered nutrient dynamics, are likely contributors. In the SCB, Ruiz-Cooley et al. (2017) documented high variability in $\delta^{15}N$ values of source- and trophic- amino acids using the short-beaked common dolphin (*Delphinus delphis*), as the ecosystem indicator, revealing a strong response of pelagic food webs to oceanographic disturbances as ENSO and climate change.

In the present study, we quantified $\delta^{13}C$ values from bulk tissue and individual AAs of the same predator, D*. delphis,* previously measured by Ruiz-Cooley et al. (2017) to reconstruct inter-annual changes in the carbon sources in the SCB. Specifically, $\delta^{13}C$ values of EAAs produced by the phytoplankton community, where D. *delphis* forage, from 1991 to 2008, were analyzed. Because the carbon cycle has a central role in biogeochemical cycling, climate, and greenhouse CO_2 in the atmosphere (Falkowski et al., 2000), tracking interannual variation in the $\delta^{13}C$ values of EAAs has important implications for understanding how shifts in primary production influence the SCB food web over time. Because temperature, dissolved inorganic carbon, coastal upwelling, and primary productivity are key drivers of the marine carbon cycle (Rau et al., 1996; Tagliabue & Bopp, 2008; Wu et al., 2019), we can evaluate their relative influences on temporal variability in $\delta^{13}C$ values of dolphin EAAs. This study provides a novel perspective on how long-term oceanographic variability and shifts in phytoplankton community composition are recorded in the $\delta^{13}C$ of EAAs in dolphins, offering new insights into the role of top predators as sentinels of ecosystem change in the CCS.

1.1 Hypothesis

Temporal variability in $\delta^{13}C$ values of EAAs in dolphin skin reflects environmental changes in the Southern California Bight. Lighter $\delta^{13}C$ EAAs values are expected during cold, productive periods characterized by high chlorophyll *a* concentrations and strong upwelling. During these times, CO_2 exchange between the atmosphere and ocean is enhanced and mixing with subsurface waters that

have depleted $\delta^{13}C$ DIC values due to remineralization as depth increases. Therefore, phytoplankton incorporates lighter carbon isotopes into their biomass, which is then reflected in the $\delta^{13}C$ values of EAAs in dolphins. In contrast, heavier $\delta^{13}C$ EAAs values are expected during warmer periods with weak upwelling and a stratified water column.

1.2 Objectives

1.2.1 Main objective

Evaluate interannual variability from 1990 to 2008 of $\delta^{13}C$ values of essential amino acids from common dolphins (*Delphinus delphis*) as indicators of changes in carbon fixation in relation to temperature, phytoplankton productivity, dissolved inorganic carbon, and coastal upwelling transport index in the Southern California Bight.

1.2.2 Specific objectives

Analyze time series of temperature, primary productivity (using Chl-*a* as proxy), dissolved inorganic carbon, and coastal upwelling transport index from 1990 to 2008 in Southern California Bight and describe patterns of variation.

To assess how environmental variability influences the $\delta^{13}C$ values of essential amino acids in dolphin skin and evaluate their potential as indicators of isotopic values produced by the phytoplankton community.

Chapter 2. Methodology

2.1 Study area

The Southern California Bight (Figure 1) is a region that includes coastal southern California, the Channel Islands, and the local portion of the Pacific Ocean. This region is influenced by the California Current (CC), the California Undercurrent (CU), and the Southern California Countercurrent (SCC) (Hickey, 1979).

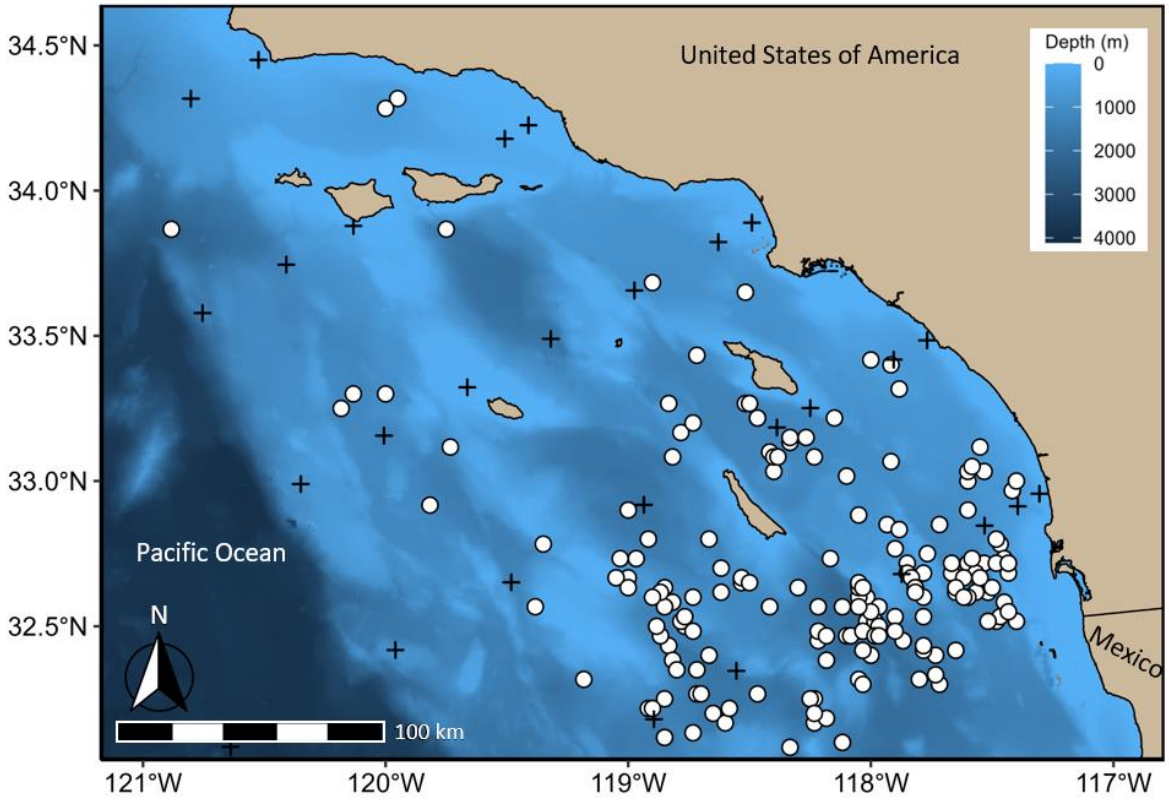

Figure 1. Map of Southern California Bight and sampling sites of *Delphinus delphis* represented with white dots; black crosses represent CalCOFI stations**.**

The study area is delimited by the coordinates 32 and 34.5 °N and 121 and -117 °W. This quadrant comprises 29 stations where CalCOFI conducts samplings four times a year (black crosses in Figure 1).

2.2 Sample collection

Skin samples of common dolphins (*Delphinus delphis*, n = 213) were collected from incidentally killed individuals from the drift and small mesh gillnet fisheries in Southern California Bight from 1990 to 2008 (Figure 2). These samples were previously analyzed by Ruiz-Cooley et al. 2017 and 2021, who focused on nitrogen and carbon isotope analysis of bulk tissue and $\delta^{15}N$ of individual AAs. It was observed that females and males as well as adults and juveniles did not show differences in the isotopic niches of $\delta^{13}C$ and $\delta^{15}N$, therefore, it is proposed that due to being highly social, they share the same habitat and feed on similar prey, in addition to recognizing intraspecific cooperative behavior as a feeding success strategy (Ruiz-Cooley et al., 2021). Based on this, it was decided to eliminate the offspring since they are isotopically different due to their dependence on maternal milk, and the analysis is focused on animals that feed on the ecosystem. Unpublished isotopic carbon data of individual amino acids from Ruiz-Cooley were used in the present study.

2.3 Bulk Carbon Stable Isotope Analysis

Of the 213 dolphin samples, 35 originating from calves were excluded, so data from adults were used, as they consume epipelagic and mesopelagic prey in the SCB and integrate primary producer values from the habitat where this species forages. Evidence from stomach content analysis revealed that the diet of *D. delphis* in SCB is dominated by squid, with *Abraliopsis* spp. as the most important prey, followed by *Gonatus* spp. Lanternfishes (Myctophidae) are also significant, with seven species among the top twelve prey items. Most other fish, including coastal pelagics as Pacific hake, jack mackerel, Pacific saury, northern anchovy, Pacific mackerel, and sardine, were of minor importance (Preti, 2020).

The $\delta^{13}C$ values were quantified in 178 samples of bulk skin from different adult dolphin individuals. All samples were stored frozen without any preservative at – 20°C. Skin tissue samples were lipid extracted with petroleum ether using the accelerator solvent extractor (ASE system). Skin samples were analyzed by using an isotope ratio mass spectrometer (IRMS, Thermo Finnigan Delta Plus), and $\delta^{13}C$ from bulk skin tissues was obtained for each sample. Isotope ratios are expressed in standard notation (equation 1):

$$\delta^{13}C = [(R_{sample}/R_{standard})-1] \times 1000 \quad (1)$$

where R_{sample} is the ratio of $^{13}C_{sample}/^{12}C_{sample}$ and $R_{standard}$ is the ratio of $^{13}C_{standard}/^{12}C_{standard}$ (Vienna Pee Dee Belemnite (VPDB) is the international standard for carbon).

2.4 Carbon CSIA of Amino Acids

From the set of bulk tissue samples, a total of 30 samples were randomly selected for compound-specific stable isotope analysis (CSIA) of individual amino acids AAs. The $\delta^{13}C$ values of individual AAs were quantified from 30 skin samples from 1990 to 2008 (two samples per year, except for 1990, 1992, 1994, 1999, 2001, 2004, 2006, 2007 with only one sample). EAAs and NEAAs were quantified following modified established protocols (Styring et al., 2012; Walsh et al., 2014).

Concisely, 2 mgs of lyophilized and well-homogenized skin tissue were dissolved in 6N HCl, placed into amber vials, flushed with N_2, sealed, and hydrolyzed in an oven at 150 °C for 70 min. Samples were dried at 60 °C under a gentle flow of N_2, the remaining solids were re-suspended in 0.4 M HCl and stored at -20 °C until derivatization. Prior to derivatization, an internal reference material, L-norleucine, dissolved in 0.4M HCl, was added to the hydrosylates, followed by methanol and pyridine. Finally, methyl chloroformate (derivatizing reagent) was added, and the solution was vortexed for 30 seconds. After ten minutes, chloroform was added and vortexed again. The organic layer was removed, dried over sodium sulfate, and re-suspended in chloroform prior to analysis.

The $\delta^{13}C$ values were measured by gas chromatography-combustion isotope-ratio mass spectrometry (GC-C-IRMS). CSIA of AAs was performed on a Thermo Trace gas chromatograph coupled to a Delta V Advantage IRMS via a GC IsoLink combustion interface (Thermo Electron, Bremen, Germany). During measurement, provisional values were calculated by comparison to a pure reference gas (N_2). Each sample was run twice to observe variability among chromatograms and obtain individual AAs $\delta^{13}C$ values.

2.5 Environmental variables

Time series of environmental variables were constructed to evaluate patterns of temporal variation in $\delta^{13}C$ values of EAAs in relation to changes in the environment. We selected four environmental variables that are likely to influence the isotopic variation of EAAs: water column temperature, primary productivity (Chl-*a* as a proxy), dissolved inorganic carbon (DIC) concentration, and a coastal upwelling transport index (CUTI).

2.5.1 Temperature

Sea water column temperature (°C) data were obtained from the CalCOFI database available at: https://calcofi.org/data/oceanographic-data/bottle-database/, download date: February 2025. The temperature was averaged from 0 to 50 m depth at each station (one data point every 10 m). This average value represents the first 50 m of the euphotic zone, considering that the deep chlorophyll maximum (DCM) typically occurs around 30 meters depth (Chow et al., 2013). This depth encompasses the peak phytoplankton biomass within the euphotic zone, providing a meaningful approximation of the thermal conditions relevant to primary production. The values from all stations for that cruise were then averaged (a value representative of the season, since only four CalCOFI cruises are made per year).

2.5.2 Chlorophyll *a* (Chl-*a*)

Chl-*a* concentration (µg/L) data were obtained from the CalCOFI database available at: https://calcofi.org/data/oceanographic-data/bottle-database/, download date: February 2025. Chl-a was measured fluorometrically in seawater samples collected at CalCOFI stations. Seawater is collected from various sampling depths using 10-liter Niskin bottles attached to a 24-place CTD-Rosette frame. The Chl-*a* concentration was averaged from 0 to 50 m depth at each station (one data point every 10 m). The values from all stations for that cruise were then averaged (a value representative of the season, since only four CalCOFI cruises are made per year).

2.5.3 DIC (Dissolved Inorganic Carbon)

DIC data were obtained from the CalCOFI database (https://calcofi.org/data/oceanographic-data/dic/). There is no complete record for our study period; data are available from 1990 to 1993 only for station 90.70 from the CalCOFI, and an average value from four stations for 2008 (sampling depth ~10 m). There is another station outside our study area (i.e., 90.90), which is more oceanic, but has DIC data from 1990 to 2001. Therefore, we decided to incorporate this information as no other data was available. For the years 2002 to 2007, no records exist. The missing data were modeled as a function of water temperature using a Bayesian approach. For more details on how the missing values were calculated, see Appendix B.

2.5.4 Upwelling Index (CUTI)

The Coastal Upwelling Transport Index (CUTI) quantifies the total volume of water being upwelled or downwelled over a specified period, reflecting the vertical volume flux entering or exiting the surface mixed layer (units: volume of vertical transport per second per meter of coastline). CUTI measures the total vertical movement of water through the base of the mixed layer by combining two processes: Ekman and geostrophic transport. Ekman transport is driven by alongshore winds and wind stress curl, which causes surface waters to spread apart or converge, leading to vertical flow. Geostrophic transport results from pressure gradients along the coast that move water across the shore, also contributing to vertical movement. Together, these processes determine the overall vertical flux of water in the system. CUTI data are available at a 1˚ spatial resolution along the U.S. West Coast (31–47˚N; Jacox et al., 2018), with each grid cell extending 75 km offshore. For this study, we used data from the 33˚N bin, which aligns with the center of our study region. CUTI database is available at: https://mjacox.com/upwelling-indices/, download date: February 2025.

2.5.5 Interpolation of environmental data

To obtain a continuous daily series of environmental variables, a linear interpolation was performed on the observed data for temperature, chlorophyll concentration, upwelling index (CUTI), and dissolved inorganic carbon (DIC). To do this, a daily sequence of dates was generated, spanning from

the first to the last available record (07-1989 to 10-2008, 87 records). Subsequently, the approx() function in R (R Core Team, 2024) was used to interpolate the values of each variable on the intervening days between observations. This method assumes a linear change between successive measurements and allows for the construction of a time series with daily resolution, which facilitates the subsequent analysis of trends, seasonality, and relationships with the $\delta^{13}C$ values of the dolphin samples.

2.5.6 Time lag

The transfer time required for carbon isotopic ratios from primary producers to transfer through the food web to dolphins is not precisely known but is estimated to range from 4 to 5 months. Additionally, the isotopic half-turnover time in dolphin skin tissue is 24.16 ± 8.19 days (Giménez et al., 2016). Therefore, on average, the isotopic signal is integrated over approximately 5 to 6 months from the base of the food web to the dolphin's skin. Consistent with this estimate, Ruiz-Cooley et al. (2017) also found that a 6-month lag provided the best predictor of the isotopic signal in historical data.

Considering this, the average daily values of the environmental variables from the prior 5 to 6 months to the dolphin sampling date were calculated, starting from the dolphin sampling date. That is, a monthly average value for each of the environmental variables was assigned to each of the dolphin samples, which were subsequently compared with the isotopic values of the amino acids in each sample. Most dolphin samples were collected in winter, so applying the 5-6-month lag to the oceanographic variables corresponds to summer oceanographic conditions.

2.5.7 Anomaly calculation

To evaluate interannual variability in environmental conditions, monthly anomalies were calculated from an 18-year daily time series. Daily values were first aggregated into monthly means. A long-term monthly climatology was then created by averaging each calendar month for the entire 18-year period. Calculating anomalies reveals how much a variable´s value in a specific month deviates from its long-term average for that month, allowing us to identify unusual variations or atypical events. Anomalies were obtained by subtracting the corresponding monthly climatological mean from each monthly

mean (equation 2), effectively isolating deviations from typical seasonal conditions and highlighting anomalous environmental events.

$$A = M_{mean} - C \quad (2)$$

where A = anomaly; M_{mean} = monthly mean (month of our interest); C = Climatology (monthly mean of the entire time series), that is, the average of all the Januaries, or all the Febuaries over the 18-year time series, depending on the month of interest.

2.5.8 Database

A database is created with the 29 dolphin samples, their respective isotopic values of EAAs, and values of environmental variables for that day and the corresponding anomaly.

2.6 Statistical analysis

Descriptive statistical analyses of bulk and essential amino acid $\delta^{13}C$ values, along with environmental variables, were conducted in RStudio version 4.4.0 (R Core Team, 2024) to characterize the dataset. Normality and homogeneity of variances were assessed using Shapiro–Wilk and Bartlett tests, respectively. Boxplots were generated to visualize isotopic variation and compare patterns among amino acids. Pearson correlation matrices were then used to quantify the strength and direction of linear relationships, providing an overview of potential associations between $\delta^{13}C$ values of EAAs and environmental parameters, and guiding subsequent analyses.

To investigate potential non-linear relationships, Generalized Additive Models (GAMs) were applied to assess the temporal response in $\delta^{13}C$ EAAs values in relation to temperature, primary productivity, coastal upwelling, and DIC. GAMs extend traditional linear models by using smooth functions (“splines”) to capture complex patterns without assuming a predefined functional form, making them well-suited for ecological and oceanographic studies where relationships are often non-linear and influenced by temporal or seasonal dynamics.

Chapter 3. Results

3.1 Bulk Carbon Isotope Analysis

The $\delta^{13}C$ values of 178 bulk skin tissues of *Delphinus delphis* from 1990 to 2008 ranged from -16.38 to -20.05 ‰, with an average of -18.27 ‰ (Figure 2). The lowest variability was observed in 1998 and 2007, while the highest variability was found in 1991 and 2002 (more than 3‰). The data were normally distributed (n = 178, alpha=0.05, p>0.05) and homoscedastic (alpha=0.05, p > 0.05). An ANOVA was carried out to determine if there were differences between years. It was observed that there were no statistically significant differences between years (alpha=0.05, p>0.05).

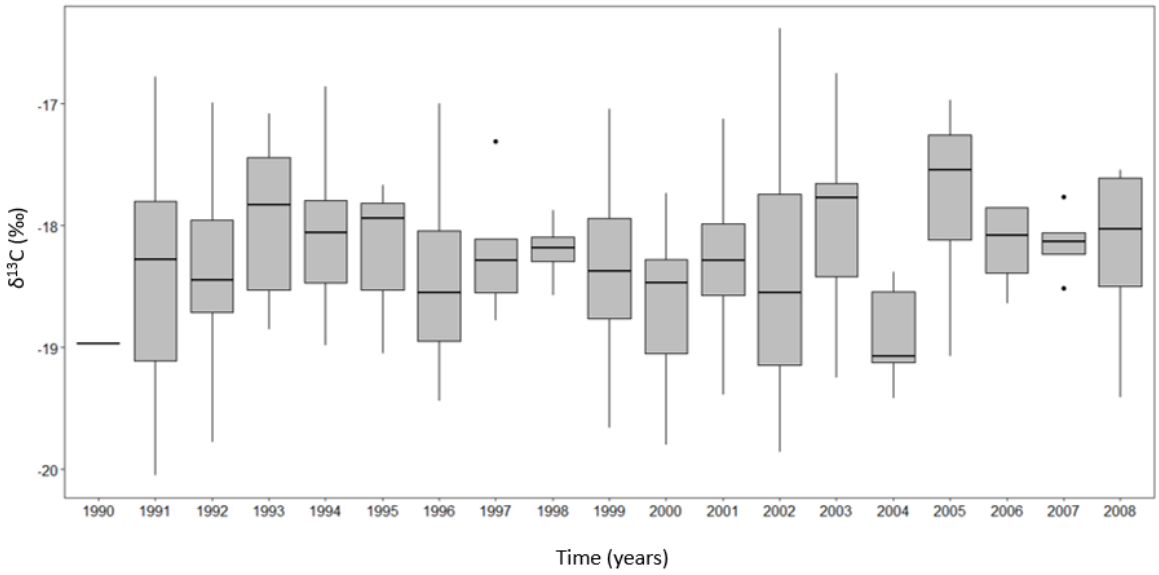

Figure 2. Boxplots of bulk $\delta^{13}C$ of skin samples of common dolphins (*Delphinus delphis*, n=178) from 1990 to 2008.

3.2 Carbon Compound Specific Isotope Analysis of Amino Acids

The $\delta^{13}C$ values of 12 individual AAs were quantified from 30 skin samples of common dolphins (Ddel) collected from 1990 to 2008 (Table 3). One sample collected in 1994 was excluded from the analysis as it represented an outlier. The outlier identification was based on the interquartile range (IQR)

method with a threshold of 1.5 × IQR, implemented in R. Of the 12 quantified amino acids, five were NEAAs: alanine (Ala), aspartic acid (Asp), glutamic acid (Glx), glycine (Gly), and proline (Pro); and seven were EAAs: isoleucine (Ile), leucine (Leu), lysine (Lys), methionine (Met), phenylalanine (Phe), valine (Val) and threonine (Thr).

Glx, Gly, Lys Phe, and Thr did not exhibit a normal distribution (alpha = 0.05, $p < 0.05$), and the data also violated homoscedasticity assumptions (alpha = 0.05, $p < 0.05$). Therefore, the nonparametric Kruskal-Wallis test (analogue of one-way analysis of variance) was use to evaluate differences between groups ($p = 2.2e^{-16}$). To identify where these differences occurred, the Wilcoxon test was used to perform pairwise comparisons between groups, with p-values adjusted for multiple comparisons using the Bonferroni method (see the matrix, Figure 10).

These results can be visualized graphically in the boxplot (Figure 3). Panel A shows bulk values, and panels B and C show the boxplots of NEAAs and EAAs, respectively (descriptive statistics in Table 4). The $\delta^{13}C$ values of individual AAs varied between -2.52‰ (Glx) to -30.42‰ (Phe). Regarding the $\delta^{13}C$ NEAAs (panel B), these show more enriched values compared to the EAAs in general, except for Thr (an essential amino acid), which has the most enriched average of all AAs (mean=-5.37 ± 1.64‰), followed by Gly and Glx (mean=-7.44 ± 3.56‰ and mean=-8.47± 3.53‰, respectively). In fact, these three AAs did not exhibit statistically significant differences according to the Wilcoxon test (Figure 10), so we could say that Thr showed greater similarity to NEEAAs than with EAAs. Gly and Glx also are the NEAAs with the greatest variability in their values (range= 11.94 and 11.18 ‰, respectively). On the contrary, Pro is the AA that had the lowest variation among AAs (range= 1.96‰).

Concerning the EAAs, Lys exhibited the highest variation (range= 10.34‰) and the second most enriched $\delta^{13}C$ values (mean=-14.66 ± 3 ‰), only below threonine (mean= - 5.37‰). On the other hand, Val is the EAA with the lowest variation (range= 2.75‰), followed by Leu (range= 3.94‰). Phe is the AA with the most depleted values among AAs (mean=-26.12 ± 1.64 ‰), followed by Met (mean=-25.91 ± 1.47‰). There were no statistically significant differences between these two EAAs (Figure 10). For detailed information on the means, maximum and minimum values, standard deviation, variance, and range of each AAs, see Table 4.

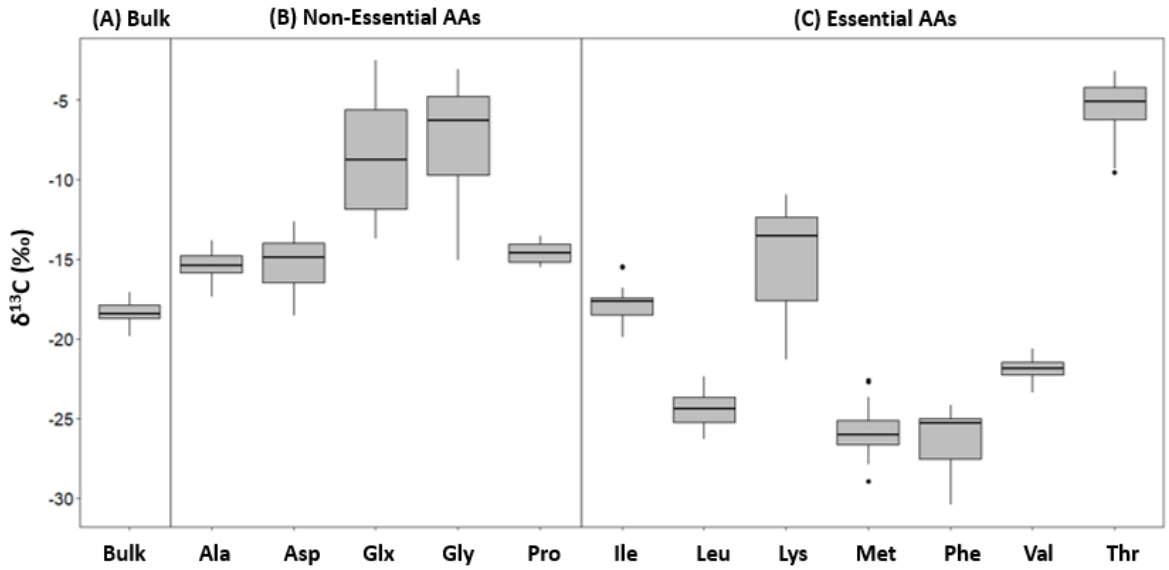

Figure 3. Boxplot of stable isotope values $\delta^{13}C$ of bulk and EAAs of skin samples of common dolphins (*Delphinus delphis*, n=29) from 1990 to 2008. (A) Bulk $\delta^{13}C$; (B) The $\delta^{13}C$ values of non-essential AAs: alanine (Ala), aspartic acid (Asp), glutamic acid (Glx), glycine (Gly), proline (Pro); and (C) The $\delta^{13}C$ values of essential-AAs: isoleucine (Ile), leucine (Leu), lysine (Lys), methionine (Met), phenylalanine (Phe), valine (Val), and threonine (Thr).

3.3 Temporal Trends of EAAs

A time series was constructed by plotting $\delta^{13}C$ values of EAAs against sampling years to examine temporal patterns (Figure 11). To evaluate the general temporal trends in the $\delta^{13}C$ values of EAAs, simple linear regressions were performed using year as the predictor variable (Figure 12). This approach allows us to assess whether each amino acid showed a significant increase or decrease over time. The goal was to identify long-term patterns of isotopic variation potentially linked to environmental or ecological changes.

The linear regression analysis revealed distinct temporal patterns in $\delta^{13}C$ values among the EAAs (Figure 12). Specifically, Lys, Met, and Phe showed statistically significant decreasing trends over time, indicating a gradual decline in their $\delta^{13}C$ values. Conversely, Leu exhibited a significantly increasing trend. In contrast, Val, Thr, Ile, and the overall mean of EAAs did not demonstrate significant temporal trends. The adjusted R^2 values for these models were very low to moderate (Table 5), suggesting that while time explains part of the variation in $\delta^{13}C$ values, other environmental or biological factors likely contribute substantially.

A smoothed trend line (using a locally weighted regression, or LOESS) was plotted to better visualize short-term fluctuations and non-linear patterns in $\delta^{13}C$ values over time (Figure 4). This allowed for a more detailed examination of potential variations not captured by the linear model.

Leu, Lys, and Phe had the most enriched $\delta^{13}C$ values in 2002. Lys and Phe exhibited lower $\delta^{13}C$ values after 2002; their most depleted $\delta^{13}C$ values occurred in late 1998. Ile and Met exhibited similar patterns, with a positive peak in 1996 and a general trend toward lighter values thereafter; however, this shift was more pronounced in Met. Thr did not show a clear trend, although the notably low values in 1997 and 2004 stood out. Val also showed no clear temporal pattern.

Regarding the ranges of variations, notable differences among AAs were evident. Val exhibited the least variation, fluctuating by only 2‰ throughout the time series, while Lys showed much greater variability, with fluctuations of up to 10‰. The remaining EAAs displayed intermediate variability, ranging between 3‰ and 6‰. All AAs $\delta^{13}C$ values were plotted using a uniform y-axis scale of 8‰, except for Lys, for which this was not feasible due to its high variability.

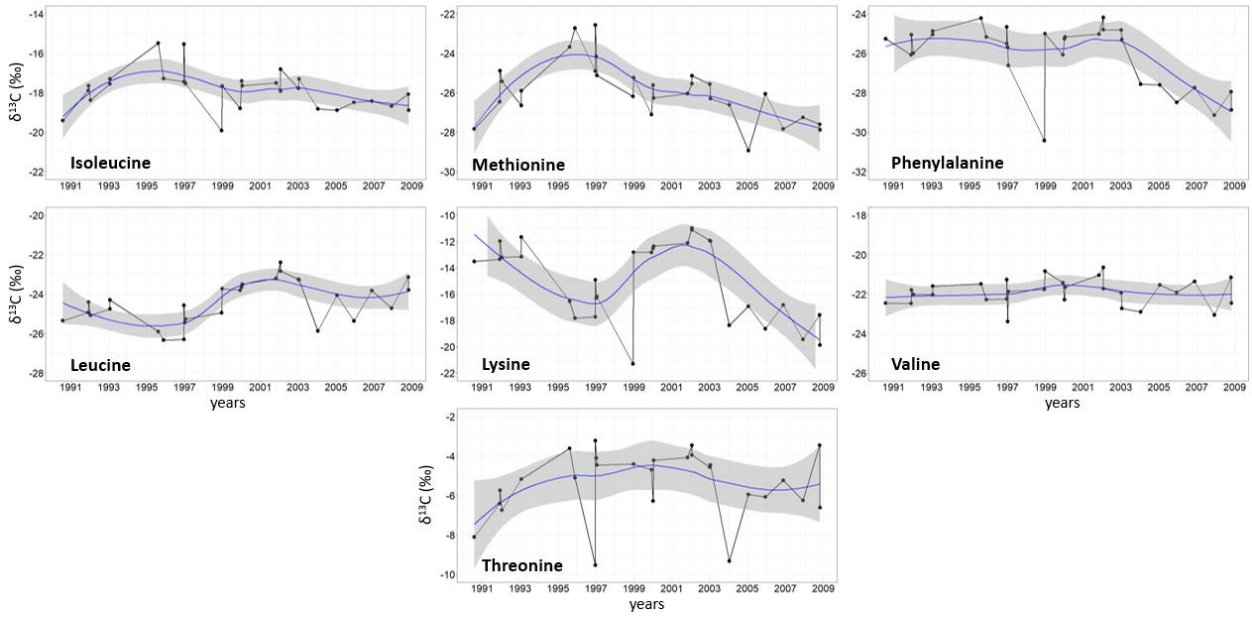

Figure 4. Time series of $\delta^{13}C$ values for each EAA in skin samples of common dolphins (*Delphinus delphis*) from 1990 to 2008. A smooth tendency blue line was added. The gray shade represents the 95% confidence interval. Every black dot represents the dolphins' capture date.

3.4 Environmental variables

Time series of temperature (average value from 0 to 50 m depth), and primary productivity (using Chl-*a* as a proxy, average value from 0 to 50 m depth), dissolved inorganic carbon (DIC) and the coastal upwelling transport index (CUTI) were constructed to understand patterns of temporal variation in $\delta^{13}C$ values of EAAs of common dolphin's skin samples in relation to changes in the environmental from 1990 to 2008 (Figure 5). Each panel presents the monthly anomalies of a given variable, calculated relative to the long-term climatological mean (indicated by the dashed horizontal line at zero). This approach emphasizes deviations from baseline conditions, enabling the identification of interannual to decadal variability and potential regime shifts.

Column water temperature anomalies exhibit moderate interannual variability throughout the study period. The most pronounced positive anomaly occurs around 1998–1999, exceeding +2.5 °C and reflecting a strong warming event associated with a major *El Niño*. Before this, temperature anomalies fluctuated modestly around the mean. After 2000, most years show negative anomalies. For Dissolved Inorganic Carbon (DIC), a pronounced negative phase is observed from 1991 to 1994, with anomalies dropping below −10 µmol/kg. A recovery phase began in the mid-1990s, transitioning to predominantly positive anomalies after 1999. From 2000 onwards, DIC has remained consistently above the long-term average. At first glance, an inverse relationship between temperature anomalies and dissolved inorganic carbon can be detected. To determine the strength of this relationship, a linear regression was performed with an R^2 of 0.28 (Figure 13).

This indicates a significant, but not very strong, linear relationship. Regarding primary productivity, Chl-*a* concentrations display negative anomalies from 1990 to 1994, followed by a slight increase from 1995 to 1997. Two major peaks are evident, one in 1999 and another around 2001. From 2000 onwards, Chl-*a* has remained consistently above the mean in most years.

The CUTI series reflects short-term oceanographic dynamics and appears less influenced by long-term trends compared to the other variables, although it may indirectly contribute to observed variations in DIC and Chl-*a*.

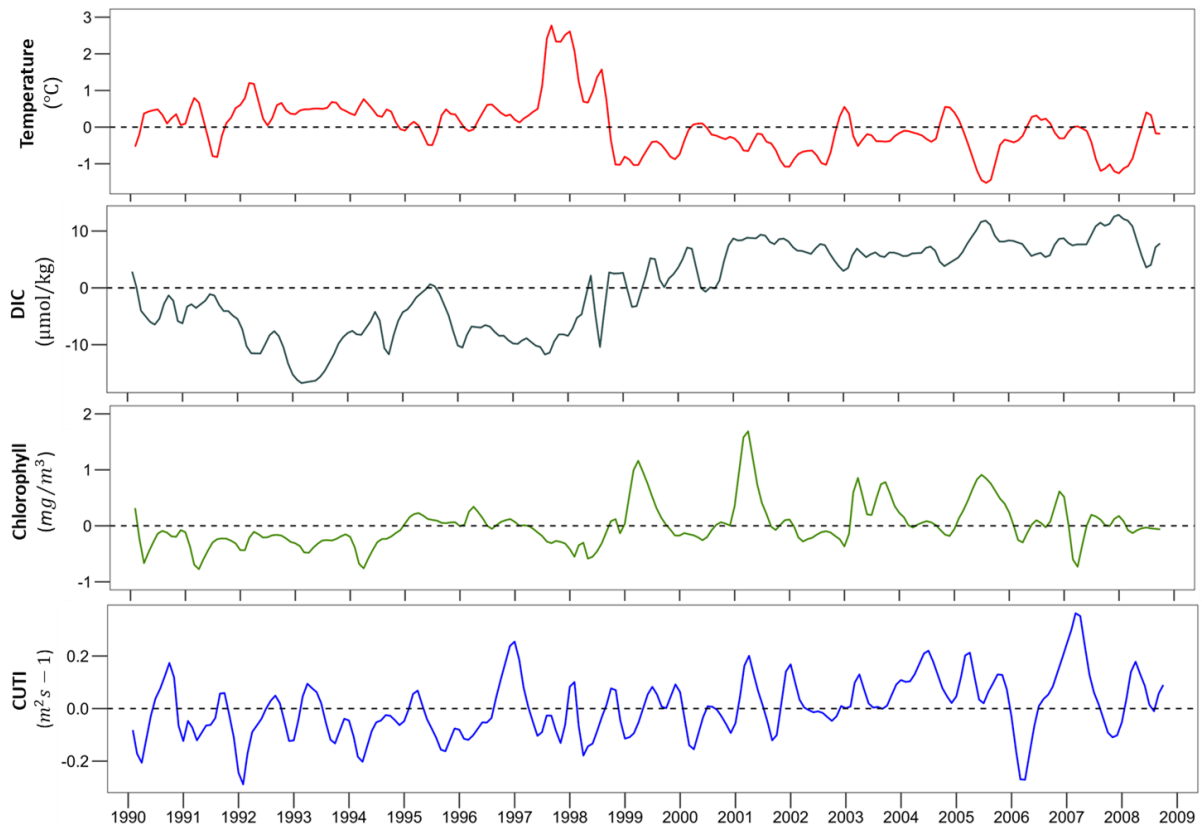

Figure 5. Time series of environmental variables. Data on temperature, Chl-*a*, and DIC were obtained from the CalCOFI database available at https://calcofi.org/data. Data of CUTI were obtained from https://mjacox.com/upwelling-indices**.** Solid lines represent monthly anomalies of a given variable, calculated relative to the long-term climatological mean. Abbreviations: dissolved inorganic carbon (DIC), coastal upwelling transport index (CUTI).

Similar to the previous graph, Figure 6 presents temporal trends in environmental variables, but this time includes a six-month lag, along with $\delta^{13}C$ values of Phe and the average $\delta^{13}C$ values of Phe, Met, Leu, and Lys. Each point corresponds to the date of dolphin capture. The $\delta^{13}C$ trend for Phe closely mirrors that of the average for Phe, Met, Leu, and Lys of $\delta^{13}C$ values. The pattern reveals a slight enrichment in $\delta^{13}C$ after 2000, followed by a sharp decline around 2003–2004, and then consistently lighter values through 2008.

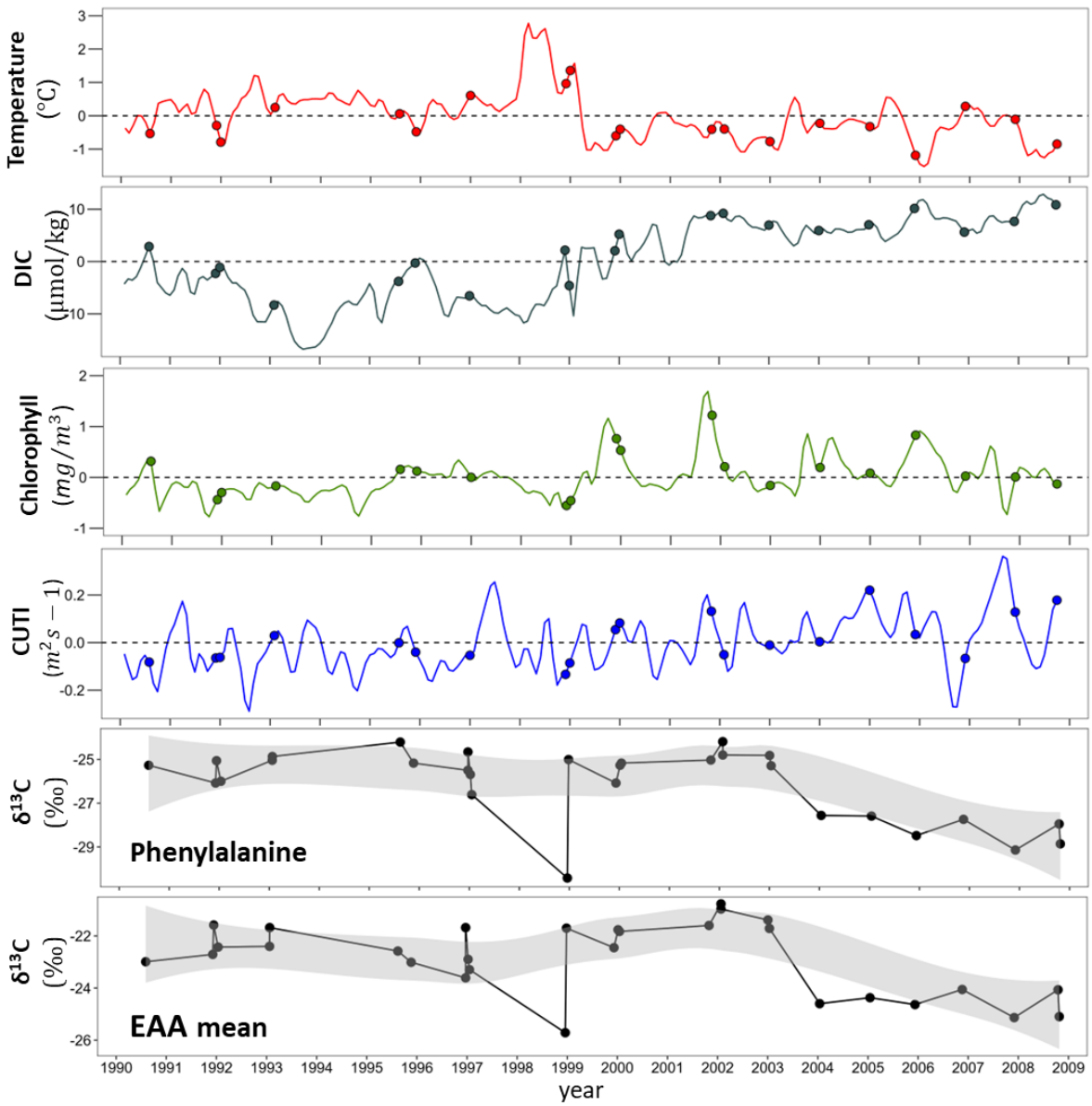

Figure 6. Time series of environmental variables, same as Figure 5 but including 5-6 months lag and $\delta^{13}C$ values of phenylalanine and $\delta^{13}C$ EAAs (mean of Phe, Met, Leu, and Lys $\delta^{13}C$ values). Dots represent the dolphins' capture date. Data on temperature, Chl-*a*, and DIC were obtained from the CalCOFI database available at https://calcofi.org/data. Data of CUTI were obtained from https://mjacox.com/upwelling-indices**.** Solid lines represent monthly anomalies of a given variable, calculated relative to the long-term climatological mean. Abbreviations: dissolved inorganic carbon (DIC), coastal upwelling transport index (CUTI).

3.5 Correlation matrix

A Pearson correlation matrix was constructed using standardized data for all $\delta^{13}C$ values of the EAAs and the environmental variables, as an initial step to explore their relationships (Figure 7). Four of the

seven EAAs showed a strong and significant correlation ($r > 0.30$) with dissolved inorganic carbon (Met, Phe, Ile, and Leu), while only methionine showed a correlation with the upwelling index. When comparing amino acids, lysine and phenylalanine showed the highest correlation ($r = 0.80$), followed by isoleucine with methionine ($r = 0.74$), and isoleucine with phenylalanine ($r = 0.71$).

3.6 General Additive Models (GAM)

To evaluate the nonlinear relationship between environmental variables and the $\delta^{13}C$ values of EAAs, Generalized Additive Models (GAMs) were applied. GAMs are a flexible extension of linear models that allow for the modeling of non-linear relationships between a response variable and one or more predictors. For each amino acid, 12 GAM configurations were tested (see models in Table 6).

The first five models included the amino acid as the response variable and each environmental variable separately, along with a time index representing the temporal structure of the data. The remaining models combined different environmental variables in various configurations. The results of each of the models were summarized in tables (Table 7). From these results, the amino acids that presented the best fit, given by the AIC and R^2 values, were selected and presented in Table 1.

Table 1. Best-Fitting GAM Models.

AA	AIC	R^2
Phe	47	0.91
Lys	102	0.85
Leu	49	0.80
Met	69	0.80

Abbreviations: amino acid (AA), Akaike Information Criterion (AIC), and coefficient of determination (R^2).

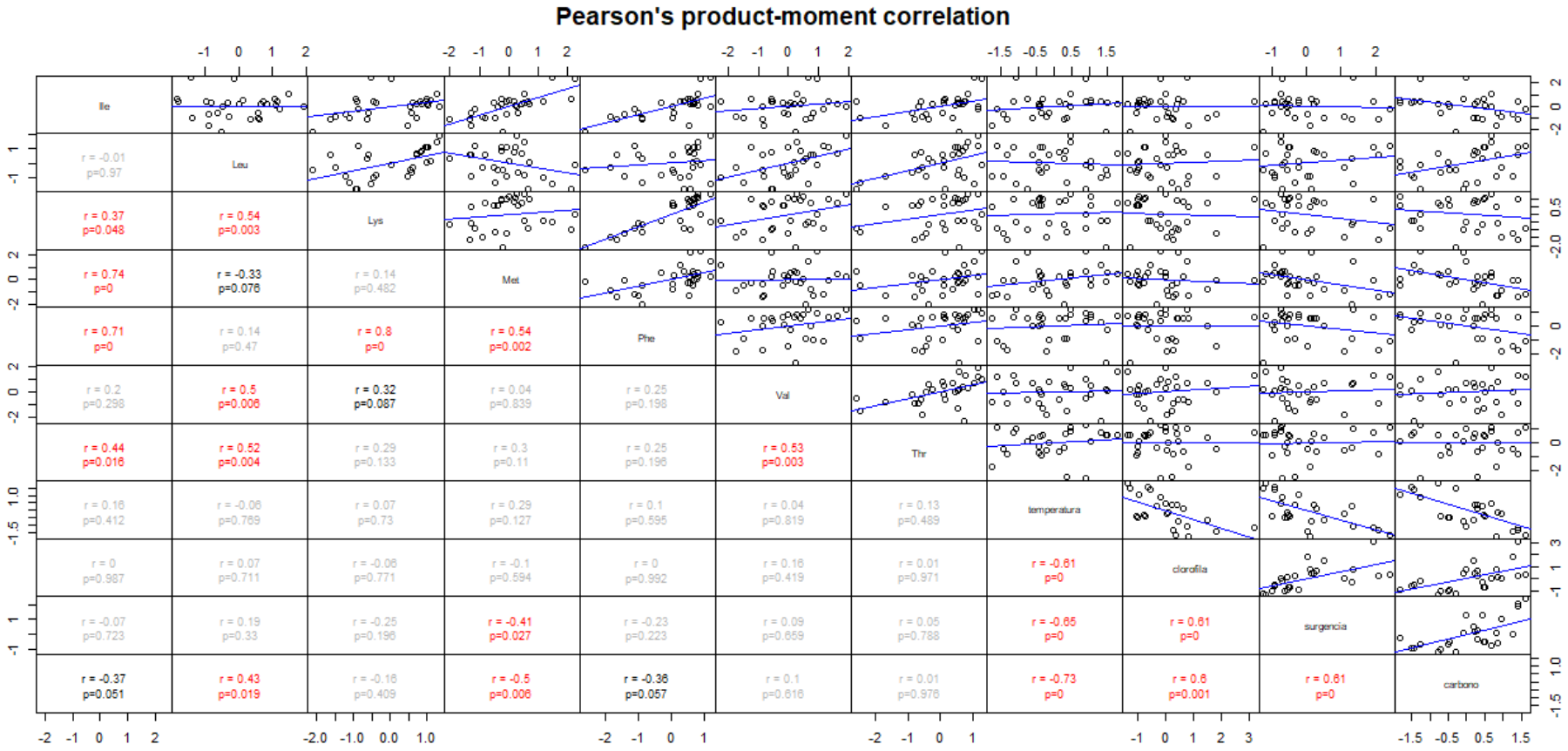

Figure 7. Correlation matrix between environmental variables and $\delta^{13}C$ values of EAA.s. All data were standardized.

Subsequently, the average isotopic values of these four amino acids were calculated, and three GAM models were run (Table 2).

Table 2. Summary of the General Additive Models in common dolphins $\delta^{13}C$ EAAs mean from the Southern California Bight, U.S.

Model	Description	AIC	R^2
Model 1	mean ~ s(time_index)+ s(Temp.) + s(DIC)	73.5	0.73
Model 2	mean ~ s(time_index)+ s(Temp.) + s(DIC) + s(Chl-*a*)	69.5	0.76
Model 3	mean ~ s(time_index)+ s(Temp.) + s(DIC) + s(Chl-*a*)+ s(CUTI)	70.1	0.76

Abbreviations: temperature (Temp), chlorophyll a (Chl-*a*), dissolved inorganic carbon (DIC), coastal upwelling transport index (CUTI), average of Phe, Lys, Leu, and Met $\delta^{13}C$ values (mean), Akaike's Information Criterion (AIC), and coefficient of determination (R^2).

The best model is number 2, which includes the temporal index, temperature, dissolved inorganic carbon, and chlorophyll a. The model explains 76.3% of the variation of $\delta^{13}C$ EAA mean. The most detailed summary of the statistical results of this model can be seen in Table 8. The model indicates that $\delta^{13}C$ EAAs mean varies nonlinearly with time, temperature, and carbon, and linearly with chlorophyll. All these effects are statistically significant, suggesting that environmental variation in these variables significantly influences the isotopic values of EAAs. The estimated effect of each predictor on $\delta^{13}C$ values is shown in Figure 8. The horizontal axis represents the observed range of each

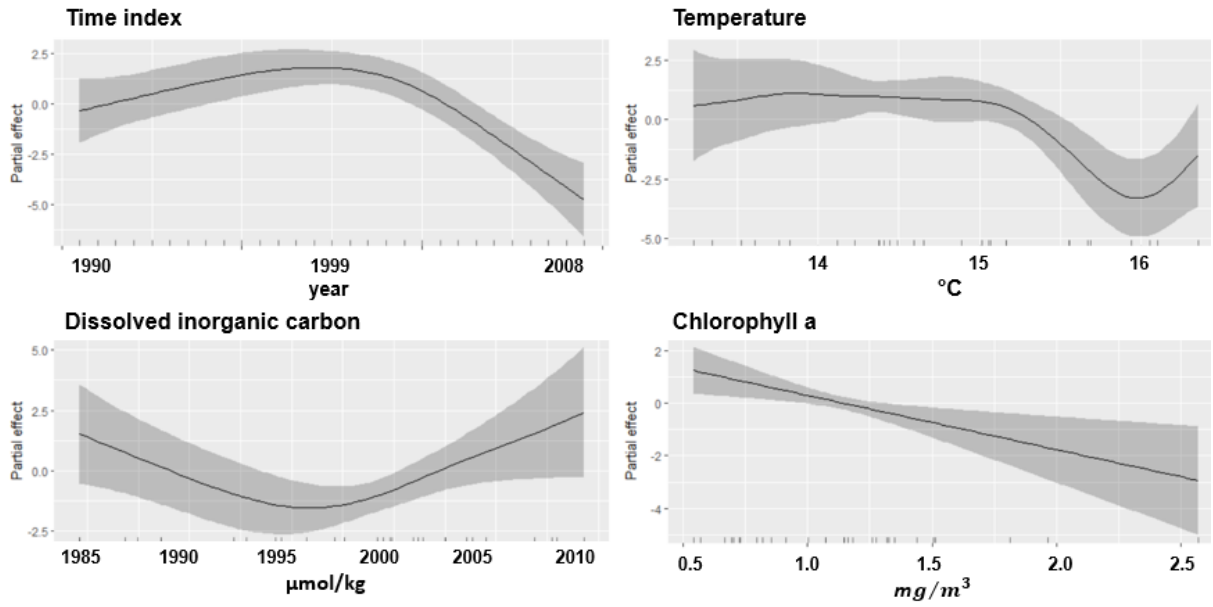

Figure 8. Resultant trends of $\delta^{13}C$ EAAs mean in response to the effect of each environmental variable using General Additive Models, and assuming the other variables remain constant.

variable, and the vertical axis shows the expected change in $\delta^{13}C$ EAAs mean in response to that variable, holding all other variables constant. The solid line is the GAM-fitted relationship, while the shaded band corresponds to the 95% confidence interval.

The analysis of each predictor variable revealed distinct patterns in relation to the $\delta^{13}C$ EAAs mean. The temporal trend, represented by the Time index, exhibited an inverted U-shape. The $\delta^{13}C$ values increased slightly during the first half of the series (1990–1998), reached a peak around 1998, and then declined toward 2008. The narrow confidence interval indicates high certainty in this pattern, highlighting a significant non-linear temporal effect that may reflect changes in carbon sources or oceanographic conditions over time.

Temperature showed a gentle, U-shaped relationship with $\delta^{13}C$, which is relatively weak. Within the 13.5–15.5°C range, the effect was nearly flat or slightly negative, while above 16°C, the effect appeared to become positive, although with increasing uncertainty at the extremes. This suggests a subtle, non-linear influence of temperature, with a potential minimum around 15.8°C. Dissolved inorganic carbon exhibited a more pronounced U-shaped pattern. Negative effects on $\delta^{13}C$ EAAs mean were observed until approximately 1995, after which the relationship shifted toward positive values. Intermediate DIC values tended to deplete $\delta^{13}C$, whereas extremely low or high values produced more positive effects. Chl-*a* displayed a clear negative linear relationship with $\delta^{13}C$ EAAs mean. Higher Chl-*a* concentrations, which serve as a proxy for primary productivity, correspond to lighter $\delta^{13}C$ values.

Chapter 4. Discussion

4.1 Bulk Carbon Isotope Analysis

Delphinus delphis typically follows a relatively constant distribution range, suggesting that the overall foraging areas remain relatively constant due to site fidelity and recurrent use of specific ocean zones (Ball et al., 2017). In the SCB, common dolphins use both coastal and oceanic regions based on visual sighting (Douglas et al., 2014; Henderson et al., 2014; Campbell et al., 2015). Hence, D. *delphis* integrates and reflects the isotopic composition of phytoplankton from this overall large region in Southern California, supporting the use of the CalCOFI data to investigate temporal trends. Since $\delta^{13}C$ in marine consumers primarily reflects primary producer values (Peterson and Fry, 1987), the lack of significant differences in bulk $\delta^{13}C$ values of D. *delphis* skin between years suggests relative stability in the main carbon sources throughout the study period (1990–2008).

This stability suggests that despite SCB being an ecosystem with high seasonal oceanographic variability, such as upwelling and interannual climate oscillations like ENSO (McClatchie, 2014), no drastic changes in phytoplankton isotopic composition occurred during the study period. This is consistent with previous observations showing no major variations in phytoplankton biomass or community structure (Venrick, 2012). Likewise, multidecadal records of zooplankton $\delta^{15}N$ (commonly used to investigate variability in the nitrogen cycle despite accruing trophic effects) demonstrate that baseline values have remained constant over decades, with some fluctuations associated with specific climate anomalies (Ohman et al., 2012). For example, during the 1998 *El Niño*, a $\delta^{15}N$ enrichment of approximately 2‰ was measured across all AAs and zooplankton groups, and values quickly returned to their previous values in 1999 during the La Niña event (Décima et al., 2013).

Stable isotope analysis of carbon in bulk tissue, however, may fail to detect subtle interannual variations in the carbon source because it integrates the total isotopic signal of all compounds present in the tissue (proteins, lipids, and carbohydrates), without distinguishing among them or accounting for their different metabolic pathways (Post, 2002; Fry, 2006). This limitation is particularly relevant in dynamic marine environments, where short-term environmental shifts may not be captured in bulk tissue values. Conversely, the results of $\delta^{13}C$ EAAs measured from predators resident from a given

ecosystem are expected to reveal carbon baseline shifts (Ruiz-Cooley et al. 2014) considering that EAAS can be synthesized only by primary producers (Larsen et al., 2013)

4.2 Carbon CSIA of Amino Acids

The $\delta^{13}C$ values of EAAs and NEAAs were consistently distinct and exhibited substantial variability within each group (Figure 3). Overall, NEAAs tended to be more enriched in ^{13}C than EAAs, in agreement with the general expectation that NEAAs reflect a mixture of primary production sources and metabolic routing from dietary carbon, whereas EAAs preserve the isotopic composition of the primary producers at the base of the food web (McMahon et al., 2010). An interesting exception to this general pattern was Thr, an EAA that exhibited the most enriched $\delta^{13}C$ mean value among AAs, clustering isotopically with NEAAs rather than with other EAAs. Similar deviations for $\delta^{13}C$ values of Thr have been reported in other marine consumers. Notably, in beluga whales, Thr $\delta^{13}C$ values differed significantly between skin and muscle tissues, suggesting that tissue-specific turnover rates or post-synthetic modifications may contribute to its enriched $\delta^{13}C$ mean value (Matthews et al., 2024). These authors suggested that Thr should be used with caution in EAA studies due to its variable $\delta^{13}C$ values.

Recall, the biosynthesis of EAAs occurs exclusively in primary producers, and once transferred throughout the food webs, their $\delta^{13}C$ values change very little ($\Delta C < 1‰$) (DeNiro & Epstein, 1978). This stability has been confirmed in both controlled experiments and field studies across various systems, including algae–copepod–fish (Liu & Cai, 2017), sponge–sea slug (Takizawa et al., 2020), and penguin–herring food chains (McMahon et al., 2015a). Therefore, the $\delta^{13}C$ values of EAAs measured in dolphins should reflect the average value of the biosynthetic pathways of the original primary producers integrated over a period. The AAs isotopic fractionation patterns would depend on the characteristics of the phytoplankton community (e.g., composition, size, and biomass) and the environmental conditions under which carbon was fixed.

Within the EAAs, Lys displayed the highest $\delta^{13}C$ variability (up to 10 ‰), which may be linked to its distinctive metabolic routing. Because the carbon skeleton of Lys is routed through metabolic pathways with limited exchange into the central carbon pool (e.g., pyruvate or α-ketoglutarate intermediates; O'Connell, 2017), it may retain its original $\delta^{13}C$ values from the phytoplankton community. Consequently, Lys may reflect shifts in the isotopic composition of primary producers

directly, and with greater amplitude, than other AAs whose carbon skeletons are more extensively scrambled through central metabolism.

This is consistent with $\delta^{13}C$ values of individual AAs in marine organisms because EAA, particularly Lys, Phe, and Thr, reflect $\delta^{13}C$ values from autotrophs that supported the food web where animals feed (Larsen et al., 2020, Yun et al., 2022). Such $\delta^{13}C$ values of EAAs are minimally influenced by animal metabolism and trophic steps, as demonstrated in controlled feeding experiments (McMahon et al., 2015b; Liu & Cai, 2017). These patterns were confirmed in the field using complex samples from estuaries and samples of pelagic predators where the unique EAAs $\delta^{13}C$ values allowed to discriminate the main carbon sources (Larsen et al., 2013). Therefore, the EAAs $\delta^{13}C$ values quantified from each dolphin skin sample reflect a 6-month average $\delta^{13}C$ value of the phytoplankton community prior to collection. These EAAs isotope values are expected to be sensitive to major ecological shifts in the physical environment (especially DIC, given that CO_2 is essential for photosynthesis), nutrient regimes, and changes in the composition and biomass of the phytoplankton community.

Val, Leu, and Ile exhibited much narrower isotopic variation (~ 3‰). These AAs are branched-chain EAAs (BCAAs) and are characterized by highly conserved metabolic pathways, which likely explain their relatively low variability compared to other EAAs (Takizawa, 2020). Phe and Met were the most depleted AAs, with no significant isotopic difference between them. This aligns with the well-established role of Phe as a conservative baseline tracer that undergoes minimal trophic enrichment (Larsen et al., 2013; McMahon, 2015; Sabadel et al., 2019).

The pronounced inter-AAs variability observed here likely reflects a combination of factors, including differences in metabolic routing among AAs and temporal shifts in the baseline $\delta^{13}C$ of primary producers driven by environmental variability, which will examined in greater detail below.

4.3 Temporal Trends of EAAs

Time series of EAAs $\delta^{13}C$ values varied interannually (Figure 4), except for Val, which was the only amino acid that showed no trend over time, with a variation range within 2 ‰. Some EAAs showed similar patterns among them, while others were distinct, suggesting that each AA responds differently to long-term environmental variability. Because the EAAs $\delta^{13}C$ values reflect the environmental conditions

under which carbon fixation occurred during photosynthesis (Farquhar et al., 1982), such heterogeneous patterns were expected considering that each EAAs follow different metabolic routes depending on its origin, structure, and function (Takizawa et al., 2020). Indeed, the LOESS smoothed trends (Figure 4) revealed pronounced non-linear fluctuations.

Lys, Met, and Phe showed the greatest variation in $\delta^{13}C$ values among AAs, therefore, the greatest response to environmental variability overtime (6 to 10 ‰). Thr, despite having a similar variation range to Met or Phe (6 ‰), did not show any trend. As such, no two EAAs showed the same pattern of variation, but they did share some similarities. For example, Phe, Lys, and Leu showed their most enriched values in 2002, a year in which an *El Niño* event occurred. This would be consistent with our hypothesis that during warm anomalies, higher $\delta^{13}C$ values are expected due to a decrease in CO_2 solubility in seawater, higher water column stratification, and weak upwellings that influence the phytoplankton community to incorporate more ^{13}C during carbon fixation.

Met is another EAA that showed notable variation over the time series (6‰); however, its pattern of variation is distinct. Its highest enrichment occurred in December 1997, coinciding with an *El Niño* event, which had begun in June of that year, also consistent with our hypothesis. After this point, Met showed a clear trend toward lighter values. Ile shares a similar pattern to Met, but with smother isotopic shifts (3‰).

Taken together, these results suggest that Phe, Lys, and Met, act as robust tracers of long-term baseline $\delta^{13}C$ variability, while others, such as Val and Thr, appear less reliable for this purpose. Therefore, we use the temporal trends of $\delta^{13}C$, specifically of Phe, Lys, and Met, with concurrent environmental and oceanographic records to examine which and how key environmental drivers shape the isotopic trajectories.

4.4 Environmental Variables Trends

The environmental time series reveal patterns (Figure 5) consistent with the known oceanographic dynamics of the CCS during the study period (1990-2008). One of the most documented events due to its consequences was the 1997-1998 *El Niño* (Chavez et al., 2002), which is manifested in our time series with positive water temperature anomalies above +2.5 °C at the end of 1997. In line with this,

negative anomalies were observed in DIC and primary productivity (Chl-*a*) values. Subsequently, at the end of 1998, a drastic change was observed in all environmental series, coinciding with a La Niña event, where negative water temperature anomalies, positive DIC anomalies due to an increased CO_2 dissolution rate, as well as an increase in primary productivity were present. From this point on, it is observed that the temperature in most years remains with negative anomalies, while the DIC and primary productivity maintain positive anomalies. These temporal patterns coincide with multiple records that indicate a structural change in the environmental dynamics around 1999-2000, consistent with a regime shift in the CCS (Chavez et al., 2002; McGowan et al., 2003; Peterson & Schwing, 2003). This change is associated with the negative phase of the Pacific Decadal Oscillation (PDO), which is characterized by relatively cooler sea surface temperatures on the west coast of North America, causing similar conditions observed during La Niña events (Mantua et al., 1997; Mantua & Hare, 2002).

Consistent with the oceanographic regime shift documented by Peterson and Schwing (2003), we observed (1) temperature anomalies transitioned from positive to predominantly negative values after 2000, indicating a cooler average state; (2) DIC showed a clear phase change, with persistently positive anomalies after 1999, suggesting increased inorganic carbon availability in the water column; and (3) Chl-*a* anomalies rose consistently, remaining above the mean in most years after 2000. These results are consistent with intensified upwelling and greater nutrient supply in the region during the PDO cold phase.

Although the CUTI primarily reflects short-term variability and does not exhibit a clear long-term trend, its indirect influence on phytoplankton may help explain the observed increases in both productivity and DIC. Taken together, the coherence among these variables supports the occurrence of an ecosystem regime shift in the late 1990s, with direct implications for baseline conditions influencing isotopic signals at higher trophic levels.

4.5 Variability in EAAs $\delta^{13}C$ values in response to environmental factors

Because the EAAs $\delta^{13}C$ values reflect the environmental conditions under which carbon fixation occurred during photosynthesis (Farquhar et al., 1982), they serve as reliable tracers of primary production dynamics across temporal and spatial scales, providing a record of baseline isotopic variability of the food web. The regime shifts in temperature, DIC, and primary productivity (Chl- *a*)

observed before and after 2000 (Figure 5) likely contributed to significant changes in the phytoplankton community (Venrick, 2002; 2012), which may help explain the overall higher mean $\delta^{13}C$ values prior to 2000 and the lower values observed thereafter (Figure 4).

To assess the effect of these large-scale environmental changes on the $\delta^{13}C$ EAAs composition of dolphin skin, we next explored the statistical associations between $\delta^{13}C$ values of Ess and the environmental variables**.** This analysis was conducted in two steps: first, by examining linear associations through a Pearson correlation matrix, and second, by applying GAMs to capture potential nonlinear responses. The correlation matrix (Figure 7) provided an initial overview of the associations between $\delta^{13}C$ values of EAAs and environmental variables. Several AAs, including Met, Phe, Ile, and Leu, showed significant positive correlations with DIC, suggesting that variability in baseline carbon availability may be an important driver of isotopic values. Met exhibited a positive correlation with the upwelling index, reflecting its potential sensitivity to this index. Among AAs, strong pairwise correlations (e.g., Lys–Phe, Ile–Met) suggest similar sensitivity to environmental conditions.

Because Pearson correlation only captures linear associations (Figure 7), it may overlook more complex, nonlinear relationships that are common in ecological and oceanographic systems. For this reason, the use of GAMs represents a critical step forward (Figure 8), as GAMs allow for flexible, data-driven modeling of nonlinear patterns without imposing restrictive assumptions about functional form. The GAM (Figure 9) identified the best-fitting model as one that included time index, temperature, DIC, and Chl-*a*, collectively explaining 76.3% of the variation in the $\delta^{13}C$ EAAs mean. This outcome underscores that isotopic variability cannot be attributed to a single environmental factor but rather results from the combined and potentially interacting effects of multiple drivers. Notably, the GAM framework detected nonlinear responses that were not evident in the correlation matrix alone, highlighting the added value of this modeling approach for capturing complex ecological dynamics with a nonlinear nature, offering a more ecologically realistic representation of the processes shaping EAAs $\delta^{13}C$ variation.

Assuming other variables remained constant, the estimated effect of temporal trend (with time index, as the predictor) followed an inverted U-shape (Figure 9), with $\delta^{13}C$ values peaking around 1998 and declining thereafter until 2008. This peak coincides with the strong 1997–1998 *El Niño*, while the subsequent depletion in $\delta^{13}C$ coincides with the regime shift of 1999–2000, which marked a transition toward cooler, more productive conditions. The progressive depletion in $\delta^{13}C$ EAAs after 1998 suggests

that the phytoplankton community incorporated mainly ^{12}C. The processes that may have contributed to this trend could be enhanced upwelling after the regime shift which likely increased the input of subsurface DIC, which is typically more depleted in ^{13}C compared to surface waters. Changes in phytoplankton community composition could also contribute significantly to the observed shift. The presence of large diatoms and the relative increase of dinoflagellates and smaller phytoplankton cells after 1999 (Venrick, 2012) may have contributed to lighter $\delta^{13}C$ values, as smaller cells generally exhibit higher isotopic fractionation during carbon fixation (Burkhardt et al., 1999), and smaller phytoplankton cells were overall present during warm conditions like *El Niño* 1997-98 in the SCB (Venrick, 2012).

The $\delta^{13}C$ values of EAAs were overall stable from 13 to 15 °C but a pronounced U-shaped shift of ~3‰ was documented between 15 and 16.5 °C, indicative of an important threshold in the carbon cycle of the SCB (Figure 8). After 15 °C, the $\delta^{13}C$ values decrease continuously with increasing temperatures until reaching ~ 16°C and became positive towards warmest extremes. This pattern was unexpected given that llighter EAAs $\delta^{13}C$ values were expected during cold conditions since the CO_2 exchange between the atmosphere and ocean tend to increase (Rau et al., 1997), hence, the availability of ^{12}C also increase, that should induce lower $\delta^{13}C$ values in the phytoplankton. The heavier EAAs $\delta^{13}C$ values at the warmest temperature were consistent with our initial hypothesis considering that lower CO_2 dissolution occurs in the ocean followed by weak upwellings and higher water column stratification. Interestingly, the latter pattern was only observed at extremely warm temperatures. This pattern suggests that the carbon fixed by phytoplankton community between 13 and 15 °C remains relatively constant consistent with the average mean temperature value of 14.7°C ± 1.08 (SD) over the two decades of study in the SCB. However, the presence of the strong 1997-98 *El Niño* event, that induced temperature at 17 to 19 °C (Figure. B4), likely had major effects in the community composition and size of the phytoplankton, its physiology (e.g. light inhibition), and the biochemical processes involved in the creation of metabolites like AAs.

The GAM results further highlight the strong influence of both DIC and Chl-*a* on $\delta^{13}C$ EAAs variability (Figure 9), reflecting the interplay between carbon supply and biological demand. The partial effect of DIC exhibited a U-shaped response, with depleted $\delta^{13}C$ values at intermediate concentrations (~1996 mmol/kg) and enriched values at both low and high extremes. This non-linear pattern is consistent with physiological mechanisms of phytoplankton carbon isotope fractionation, where fractionation efficiency (ε_p) depends on the balance between CO_2 availability and growth rate (Rau et al., 1997; Goericke & Fry, 1994; Laws, 1995; Burkhardt et al., 1999). At intermediate DIC, carbon is neither

limiting nor in excess, allowing cells to maximize fractionation and produce lighter isotopic signals (Rau et al., 1997). By contrast, at low DIC, carbon limitation constrains uptake, whereas at high DIC, rapid growth or reliance on bicarbonate via carbon concentrating mechanisms reduces fractionation, both resulting in enriched $\delta^{13}C$ signatures (Raven & Johnston, 1991).

Meanwhile, Chl-*a* had a consistent linear negative effect on $\delta^{13}C$ EAAs mean, suggesting that periods of elevated primary productivity were associated with lighter isotopic values. This is in agreement with our hypothesis that periods of high productivity, driven by upwelling, are associated with lighter isotopic signals. This likely reflects the preferential uptake of isotopically lighter CO_2 by phytoplankton under conditions of elevated nutrient supply and gas exchange. These pulses are likely to coincide with changes in phytoplankton community structure, favoring smaller cells with larger surface-to-volume ratios, which are known to exhibit stronger fractionation (Burkhardt et al., 1999).

After 2000, the phytoplankton community of the SCB underwent a drastic shift in taxonomic composition and bloom timing, although total chlorophyll biomass did not decline (Venrick, 2012). The seasonal peak shifted from spring to summer, accompanied by a sharp reduction in large diatoms (notably *Chaetoceros* spp.) and a relative increase in dinoflagellates and smaller phytoplankton cells. These changes suggest that while primary production levels remained relatively stable, the structure of the phytoplankton community was altered with direct implications for the use of CO_2 during the photosynthesis process and AAs synthesis.

The findings based on $\delta^{13}C$ of EAAs in common dolphins complement previous work by Ruiz-Cooley et al. (2017), who analyzed $\delta^{15}N$ of source AAs in the same dolphin time series to reconstruct temporal variation. The $\delta^{15}N$ from these AAs reflects the nitrogen sources used by phytoplankton. Source-AAs (N) and EAAs (C) both preserve the isotopic signal of primary producers, making them reliable tracers of baseline variability (Larsen et al., 2013; McMahon & McCarthy, 2016). They reflect shifts in nutrient sources of C and N and phytoplankton composition because they undergo little fractionation throughout the food web. Source-AAs $\delta^{15}N$ values showed high interannual variability and reflected changes in nitrogen assimilation by primary producers. These source-AAs $\delta^{15}N$ values were relatively higher after the 2000 regime shift indicative of higher NO_3 assimilation or a higher influence of the underwater current that bring heavier $\delta^{15}N$ NO_3 values (Ruiz-Cooley et al., 2017), while our EAAs $\delta^{13}C$ were lower after 2000. Therefore, we are finding an opposing response in the carbon and nitrogen cycles to the regime shift where the phytoplankton community is central to both biogeochemical

cycles. These variability in $\delta^{15}N$ source-AAs and our $\delta^{13}C$ EAAs trend suggest that the post-2000 changes affected both the basal isotopic signatures of primary producers (as reflected in $\delta^{13}C$ EAAs) and the vertical structure of the food web (as inferred from $\delta^{15}N$ source AAs). This dual evidence underscores the sensitivity of common dolphins to ecosystem level changes, highlighting their role as sentinels that integrate both baseline and trophic processes within the SCC.

The post-2000 restructuring of the phytoplankton community in the SCB, and its imprint on the $\delta^{13}C$ values of EAAs in common dolphins, highlights the importance of local food web pathways in determining consumer isotopic signals. However, these coastal dynamics are embedded within broader, basin-scale processes that also affect offshore ecosystems. In this study, we detected a decline in $\delta^{13}C$ values in common dolphins after 1999, a trend that is consistent with a previous study using $\delta^{13}C$ EAAs from sperm whales (*Physeter macrocephalus*), that inhabits the offshore CCS (Ruiz-Cooley et al., 2014). There a continuous decline in both $\delta^{15}N$ and $\delta^{13}C$ values was observed from 1993 to 2005 with a total shift of 3‰ for $\delta^{13}C$ EAAs. Similarly, we found that the $\delta^{13}C$ EAAs mean showed a decline of 3.5‰ starting in 2002 (Figure 7); however, this trend was not continuous, with particularly slight lower values in 2004, followed by an enrichment towards 2007, and then a decline again to milder values in 2008 (Figure 7). On the other hand, when analyzing the trend for Lys individually, it showed a variation of up to 7‰ between 2002 and 2008, making it the AA with the greatest range of variation in our study and may be the most sensitive indicator of environmental variability.

While both species exhibit isotopic depletion, the period and the magnitude of δ^{13} EAAs differ. This discrepancy suggests that the underlying mechanisms driving the carbon cycle are different for the offshore and coastal CCS, specifically the SCB. In the offshore CCS, sperm whales feed primarily on mesopelagic prey, which ultimately depends on primary production from the euphotic zone, among other biogeochemical processes that include bacterial degradation. The decline in $\delta^{13}C$ values observed in sperm whale tissues was attributed to shifts in SST, nutrient supply, and phytoplankton community structure in the outer CCS (Ruiz-Cooley et al., 2014). Such patterns are consistent with regional evidence of long-term shifts in nutrient dynamics (Bograd et al., 2008), increased stratification and shoaling of the thermocline (Palacios et al., 2004), and basin-scale climate variability, PDO and *El Niño*–Southern Oscillation (ENSO) (Chavez et al., 2002; Checkley & Barth, 2009).

The magnitude of the $\delta^{13}C$ decrease in sperm whales and dolphins EAAs exceeds what would be expected from the Suess effect alone (~0.2‰ per decade; Francey et al., 1999), indicating that regional

oceanographic processes amplify the global anthropogenic signal. The similarity in isotopic trajectories across these two distinct ecosystems suggests that $\delta^{13}C$ depletion represents a pervasive regional signal, potentially driven by the combined influence of large-scale climate forcing and global carbon cycle perturbations. Comparable declines in $\delta^{13}C$ have been reported in other marine systems and attributed to both the Suess effect and regional declines in primary productivity (Rau et al., 1989; Schell, 2001).

Common dolphins inhabit coastal habitats strongly influenced by upwellings. Specifically, the SCB is highly dynamic given the influence of mesoscale eddies, seasonal upwelling, interannual variability (ENSO), and the interplay between the California Current and Countercurrent. The decline observed in $\delta^{13}C$ EAAs values of dolphins likely reflects shifts in phytoplankton composition, particularly the increase of smaller phytoplankton in the latter half of the study period, as well as the Suess effect, although the latter alone cannot explain the magnitude of change. Variability in the intensity and timing of coastal upwelling, as documented in previous studies (Venrick, 2012; Jacox et al., 2014; Bograd et al., 2015), plays a central role as well. Unlike the relatively homogeneous offshore habitat of sperm whales possibly dominated by nano and picophytoplankton, the coastal zone is characterized by strong spatiotemporal variability, which may result in more heterogeneous temporal isotopic responses as observed in zooplankton $\delta^{15}N$ values (Ohman et al., 2012), common dolphin $\delta^{15}N$ source AAs (Ruiz-Cooley et al. 2017), and $\delta^{13}C$ EAAs of dolphins (this study).

Taken together, the comparison between sperm whales and common dolphins underscores the utility of top predators as biological sentinels of ecosystem change (Ruiz-Cooley et al. 2014, 2017, Wiley et al., 2013) and provide a finer resolution in $\delta^{13}C$ in AAs than using the bulk tissue. The consistent $\delta^{13}C$ depletion across habitats provides robust evidence of ongoing alterations in the carbon cycle within the CCS, reinforcing the value of isotopic monitoring as a tool to detect and attribute biogeochemical change in marine ecosystems.

Chapter 5. Conclusions

This study provides the first long-term reconstruction (1990–2008) of $\delta^{13}C$ values in EAAs of common dolphins from SCB, revealing that these compounds act as sensitive tracers of baseline carbon fixation under changing environmental conditions. While bulk $\delta^{13}C$ values of dolphin skin showed little interannual variation, $\delta^{13}C$ values of individual EAAs, particularly Lys, Met, and Phe, displayed pronounced fluctuations that tracked major environmental changes. These patterns highlight the stronger capacity of EAAs compared to bulk isotopes to resolve subtle but ecologically meaningful shifts in phytoplankton carbon sources.

The combined effects of DIC, Chl-*a*, and temperature indicate that $\delta^{13}C$ EAAs variability in dolphins integrates the physiological responses of primary producers to environmental change. Lighter isotopic values emerge when DIC and productivity interact to maximize fractionation, particularly under high-biomass conditions with intermediate DIC levels, whereas enriched signals occur under carbon limitation or during rapid growth with high DIC, when fractionation efficiency declines. These results underscore the value of $\delta^{13}C$ EAAs as sensitive tracers of the balance between carbon supply and demand in the SCB. The post-2000 depletion of up to 3.5‰ far exceeded the expected atmospheric Suess effect, underscoring the dominant role of regional oceanographic processes in driving isotopic variability. This study demonstrates that common dolphins function as biological sentinels, integrating carbon cycle variability across decades and offering a valuable tool to monitor ecosystem change in dynamic coastal systems.

Bibliography

Ball, L., Shreves, K., Pilot, M., & Moura, A. E. (2017). Temporal and geographic patterns of kinship structure in common dolphins (*Delphinus delphis*) suggest site fidelity and female-biased long-distance dispersal. *Behavioral Ecology and Sociobiology*, *71*(123), 1-12. https://doi.org/10.1007/s00265-017-2351-z

Bograd, S. J., Castro, C. G., Di Lorenzo, E., Palacios, D. M., Bailey, H., Gilly, W., & Chavez, F. P. (2008). Oxygen declines and the shoaling of the hypoxic boundary in the California Current. *Geophysical Research Letters*, *35*(12), 1-6. https://doi.org/10.1029/2008gl034185

Bograd, S. J., Buil, M. P., Lorenzo, E. D., Castro, C. G., Schroeder, I. D., Goericke, R., Anderson, C. R., Benitez-Nelson, C., & Whitney, F. A. (2015). Changes in source waters to the Southern California Bight. *Deep Sea Research Part II: Topical Studies in Oceanography*, *112*, 42–52. https://doi.org/10.1016/j.dsr2.2014.04.009

Bond, N. A., Cronin, M. F., Freeland, H., & Mantua, N. (2015). Causes and impacts of the 2014 warm anomaly in the NE Pacific. *Geophysical Research Letters*, *42*(9), 3414–3420. https://doi.org/10.1002/2015gl063306

Boyce, D. G., Lewis, M. R., & Worm, B. (2010). Global phytoplankton decline over the past century. *Nature*, *466*(7306), 591–596. https://doi.org/10.1038/nature09268

Breitburg, D., Levin, L. A., Oschlies, A., Grégoire, M., Chavez, F. P., Conley, D. J., Garçon, V., Gilbert, D., Gutiérrez, D., Isensee, K., Jacinto, G. S., Limburg, K. E., Montes, I., Naqvi, S. W. A., Pitcher, G. C., Rabalais, N. N., Roman, M. R., Rose, K. A., Seibel, B. A., & Telszewski, M. (2018). Declining oxygen in the global ocean and coastal waters. *Science*, *359*, 1-11. https://doi.org/10.1126/science.aam7240

Brett, M. T., Bunn, S. E., Chandra, S., Galloway, A. W. E., Guo, F., Kainz, M. J., Kankaala, P., Lau, D. C. P., Moulton, T. P., Power, M. E., Rasmussen, J. B., Taipale, S. J., Thorp, J. H., & Wehr, J. D. (2017). How important are terrestrial organic carbon inputs for secondary production in freshwater ecosystems? *Freshwater Biology*, *62*(5), 833–853. https://doi.org/10.1111/fwb.12909

Browning, N. E., Dold, C., I-Fan, J., & Worthy, G. A. J. (2014). Isotope turnover rates and diet-tissue discrimination in skin of ex situ bottlenose dolphins (*Tursiops truncatus*). *Journal of Experimental Biology*, *217*(2), 214-221. https://doi.org/10.1242/jeb.093963

Burkhardt, S., Riebesell, U., & Zondervan, I. (1999). Stable carbon isotope fractionation by marine phytoplankton in response to daylength, growth rate, and CO_2 availability. *Marine Ecology Progress Series*, *184*, 31–41. https://doi.org/10.3354/meps184031

Cai, W., Borlace, S., Lengaigne, M., Rensch, P., Collins, M., Vecchi, G., Timmermann, A., Santoso, A., McPhaden, M. J., Wu, L., England, M. H., Wang, G., Guilyardi, E., & Jin, F.-F. (2014). Increasing frequency of extreme El Niño events due to greenhouse warming. *Nature Climate Change*, *4*(2), 111–116. https://doi.org/10.1038/nclimate2100

Caldeira, K., & Wickett, M. E. (2003). Anthropogenic carbon and ocean pH. *Nature*, *425*(6956), 365–365. https://doi.org/10.1038/425365a

California Cooperative Oceanic Fisheries Investigations. (2025). Bottle *Database*. Consulted in February 2025, available at: https://calcofi.org/data/oceanographic-data/bottle-database/

Campbell, G. S., Thomas, L., Whitaker, K., Douglas, A. B., Calambokidis, J., & Hildebrand, J. A. (2015). Inter-annual and seasonal trends in cetacean distribution, density and abundance off southern California. *Deep Sea Research Part II: Topical Studies in Oceanography*, *112*, 143–157. https://doi.org/10.1016/j.dsr2.2014.10.008

Carr, M. E. (2002). Estimation of potential productivity in Eastern Boundary Currents using remote sensing. *Deep Sea Research Part II: Topical Studies in Oceanography*, *49*(1-3), 59–80. https://doi.org/10.1016/s0967-0645(01)00094-7

Cavole, L., Demko, A., Diner, R., Giddings, A., Koester, I., Pagniello, C., Paulsen, M. L., Ramirez-Valdez, A., Schwenck, S., Yen, N., Zill, M., & Franks, P. (2016). Biological impacts of the 2013–2015 warm-water anomaly in the Northeast Pacific: Winners, losers, and the future. *Oceanography*, *29*(2), 273-285. https://doi.org/10.5670/oceanog.2016.32

Chavez, F. P., Pennington, J. T., Castro, C. G., Ryan, J. P., Michisaki, R. P., Schlining, B., Walz, P., Buck, K. R., McFadyen, A., & Collins, C. A. (2002). Biological and chemical consequences of the 1997–1998 El Niño in central California waters. *Progress in Oceanography*, *54*(1), 205–232. https://doi.org/10.1016/S0079-6611(02)00050-2

Checkley, D. M., & Barth, J. A. (2009). Patterns and processes in the California Current System. *Progress in Oceanography*, *83*(1), 49–64. https://doi.org/10.1016/j.pocean.2009.07.028

Chikaraishi, Y., Ogawa, N. O., Kashiyama, Y., Takano, Y., Suga, H., Tomitani, A., Miyashita, H., Kitazato, H., & Ohkouchi, N. (2009). Determination of aquatic food-web structure based on compound-specific nitrogen isotopic composition of amino acids. *Limnology and Oceanography: Methods*, *7*(11), 740–750. https://doi.org/10.4319/lom.2009.7.740

Chow, C.-E. T., Sachdeva, R., Cram, J. A., Steele, J. A., Needham, D. M., Patel, A., Parada, A. E., & Fuhrman, J. A. (2013). Temporal variability and coherence of euphotic zone bacterial communities over a decade in the Southern California Bight. *The ISME Journal*, *7*(12), 2259–2273. https://doi.org/10.1038/ismej.2013.122

Close, H. G., & Henderson, L. C. (2020). Open-ocean minima in $\delta^{13}C$ values of particulate organic carbon in the lower euphotic zone. *Frontiers in Marine Science*, *7*, 1-10. https://doi.org/10.3389/fmars.2020.540165

Décima, M., Landry, M. R., & Popp, B. N. (2013). Environmental perturbation effects on baseline $\delta^{15}N$ values and zooplankton trophic flexibility in the southern California Current Ecosystem. *Limnology and Oceanography*, *58*(2), 624–634. https://doi.org/10.4319/lo.2013.58.2.0624

DeNiro, M. J., & Epstein, S. (1978). Influence of diet on the distribution of carbon isotopes in animals. *Geochimica et Cosmochimica Acta*, *42*(5), 495–506. https://doi.org/10.1016/0016-7037(78)90199-0

Descolas-Gros, C., & Fontungne, M. (1990). Stable carbon isotope fractionation by marine phytoplankton during photosynthesis. *Plant, Cell and Environment*, *13*(3), 207–218. https://doi.org/10.1111/j.1365-3040.1990.tb01305.x

Di Lorenzo, E., Miller, A. J., Schneider, N., & McWilliams, J. C. (2005). The warming of the California Current System: Dynamics and ecosystem implications. *Journal of Physical Oceanography*, *35*(3), 336–362. https://doi.org/10.1175/jpo-2690.1

Di Lorenzo, E., & Mantua, N. (2016). Multi-year persistence of the 2014/15 North Pacific marine heatwave. *Nature Climate Change*, *6*(11), 1042–1047. https://doi.org/10.1038/nclimate3082

Douglas, A. B., Calambokidis, J., Munger, L. M., Soldevilla, M. S., Ferguson, M. C., Havron, A. M., Camacho, D. L., Campbell, G. S., & Hildebrand, J. A. (2014). Seasonal distribution and abundance of cetaceans off Southern California estimated from CalCOFI cruise data from 2004 to 2008. *Fishery Bulletin*, *112*(2-3), 198–220. https://doi.org/10.7755/fb.112.2-3.7

Ducklow, H., Steinberg, D., & Buesseler, K. (2001). Upper ocean carbon export and the biological pump. *Oceanography*, *14*(4), 50–58. https://doi.org/10.5670/oceanog.2001.06

Falkowski, P., Scholes, R. J., Boyle, E., Canadell, J., Canfield, D., Elser, J., Gruber, N., Hibbard, K., Högberg, P., Linder, S., Mackenzie, F. T., Moore, B., III, Pedersen, T., Rosenthal, Y., Seitzinger, S., Smetacek, V., & Steffen, W. (2000). The Global carbon cycle: a test of our knowledge of Earth as a system. *Science*, 290(5490), 291–296. https://doi.org/10.1126/science.290.5490.291

Farquhar, G., O'Leary, M., & Berry, J. (1982). On the relationship between carbon isotope discrimination and the intercellular carbon dioxide concentration in leaves. *Functional Plant Biology*, *9*(2), 121-137. https://doi.org/10.1071/pp9820121

Francey, R. J., Allison, C. E., Etheridge, D. M., Trudinger, C. M., Enting, I. G., Leuenberger, M., Langenfelds, R. L., Michel, E., & Steele, L. P. (1999). A 1000-year high precision record of $\delta^{13}C$ in atmospheric CO2. *Tellus B: Chemical and Physical Meteorology*, *51*(2), 170–193. https://doi.org/10.3402/tellusb.v51i2.16269

Frölicher, T. L., Fischer, E. M., & Gruber, N. (2018). Marine heatwaves under global warming. *Nature*, *560*(7718), 360–364. https://doi.org/10.1038/s41586-018-0383-9

Fry, B. (2006). *Stable Isotope Ecology*. Springer. https://doi.org/10.1007/0-387-33745-8

Giménez, J., Ramírez, F., Almunia, J., G. Forero, M., & de Stephanis, R. (2016). From the pool to the sea: Applicable isotope turnover rates and diet to skin discrimination factors for bottlenose dolphins (*Tursiops truncatus*). *Journal of Experimental Marine Biology and Ecology*, *475*, 54–61. https://doi.org/10.1016/j.jembe.2015.11.001

Goericke, R., & Fry, B. (1994). Variations of marine plankton $\delta^{13}C$ with latitude, temperature, and dissolved CO2 in the world ocean. *Global Biogeochemical Cycles*, *8*(1), 85–90. https://doi.org/10.1029/93gb03272

Gruber, N., Keeling, C. D., Bacastow, R. B., Guenther, P. R., Lueker, T. J., Wahlen, M., Meijer, H. A. J., Mook, W. G., & Stocker, T. F. (1999). Spatiotemporal patterns of carbon-13 in the global surface oceans and the oceanic suess effect. *Global Biogeochemical Cycles*, *13*(2), 307–335. https://doi.org/10.1029/1999gb900019

Gruber, N, Keeling, C. D., & Bates, N. R. (2002). Interannual variability in the North Atlantic Ocean carbon sink. *Science*, *298*(5602), 2374–2378. https://doi.org/10.1126/science.1077077

Henderson, E. E., Forney, K. A., Barlow, J. P., Hildebrand, J. A., Douglas, A. B., Calambokidis, J., & Sydeman, W. J. (2014). Effects of fluctuations in sea-surface temperature on the occurrence of small cetaceans off Southern California. *Fishery Bulletin*, *112*(2-3), 159–177. https://doi.org/10.7755/fb.112.2-3.5

Hickey, B. M. (1979). The California current system—hypotheses and facts. *Progress in Oceanography*, *8*(4), 191–279. https://doi.org/10.1016/0079-6611(79)90002-8

Hicks, B. D., Aubin, D. J., Geraci, J. R., & Brown, W. R. (1985). Epidermal growth in the bottlenose dolphin, *Tursiops truncatus*. *The Journal of Investigative Dermatology*, *85*(1), 60–63. https://doi.org/10.1111/1523-1747.ep12275348

Hobson, K. A., Piatt, J. F., & Pitocchelli, J. (1994). Using stable isotopes to determine seabird trophic relationships. *The Journal of Animal Ecology*, *63*(4), 786-798. https://doi.org/10.2307/5256

Hoegh-Guldberg, O., Mumby, P. J., Hooten, A. J., Steneck, R. S., Greenfield, P., Gomez, E., Harvell, C. D., Sale, P. F., Edwards, A. J., Caldeira, K., Knowlton, N., Eakin, C. M., Iglesias-Prieto, R., Muthiga, N., Bradbury, R. H., Dubi, A., & Hatziolos, M. E. (2007). Coral reefs under rapid climate change and ocean acidification. *Science*, *318*(5857), 1737–1742. https://www.science.org/doi/full/10.1126/science.1152509

Hoegh-Guldberg, O., & Bruno, J. F. (2010). The impact of climate change on the world's marine ecosystems. *Science*, *328*(5985), 1523–1528. https://doi.org/10.1126/science.1189930

Jacox, M. G., Edwards, C. A., Hazen, E. L., & Bograd, S. J. (2018). Coastal upwelling revisited: Ekman, Bakun, and improved upwelling indices for the U.S. West coast. *Journal of Geophysical Research: Oceans*, *123*(10), 7332–7350. https://doi.org/10.1029/2018jc014187

Jo, N., La, H. S., Kim, J.-H., Kim, K., Kim, B. K., Kim, M. J., Son, W., & Lee, S. H. (2021). Different Biochemical Compositions of Particulate Organic Matter Driven by Major Phytoplankton Communities in the Northwestern Ross Sea. *Frontiers in Microbiology*, *12*, 1-19. https://doi.org/10.3389/fmicb.2021.623600

Keeling, C. D., Bacastow, R. B., Carter, A. F., Piper, S. C., Whorf, T. P., Heimann, M., Mook, W. G., & Roeloffzen, H. (1989). A three-dimensional model of atmospheric CO_2 transport based on observed winds: 1. Analysis of observational data. *Geophysical Monograph Series*, *55*, 165–236. https://doi.org/10.1029/gm055p0165

Kim, H.-J., Miller, A. J., McGowan, J., & Carter, M. L. (2009). Coastal phytoplankton blooms in the Southern California Bight. *Progress in Oceanography*, *82*(2), 137–147. https://doi.org/10.1016/j.pocean.2009.05.002

Kolmakova, A. A., & Kolmakov, V. I. (2019). Amino acid composition of green microalgae and diatoms, cyanobacteria, and zooplankton (review). *Inland Water Biology*, *12*(4), 452–461. https://doi.org/10.1134/S1995082919040060

Kudela, R. M., & Chavez, F. P. (2000). Modeling the impact of the 1992 El Niño on new production in Monterey Bay, California. *Deep Sea Research Part II: Topical Studies in Oceanography*, *47*(5-6), 1055–1076. https://doi.org/10.1016/s0967-0645(99)00136-8

Larsen, T., Taylor, D. L., Leigh, M. B., & O'Brien, D. M. (2009). Stable isotope fingerprinting: a novel method for identifying plant, fungal, or bacterial origins of amino acids. *Ecology*, *90*(12), 3526–3535. https://doi.org/10.1890/08-1695.1

Larsen, T., Ventura, M., Andersen, N., O'Brien, D. M., Piatkowski, U., & McCarthy, M. D. (2013). Tracing carbon sources through aquatic and terrestrial food webs using amino acid stable isotope fingerprinting. *PLOS ONE*, *8*(9), 1-9. https://doi.org/10.1371/journal.pone.0073441

Larsen, T., Hansen, T., & Dierking, J. (2020). Characterizing niche differentiation among marine consumers with amino acid $\delta^{13}C$ fingerprinting. *Ecology and Evolution*, *10*(14), 7768-7782. https://doi.org/10.1002/ece3.6502

Laws, E. A., Popp, B. N., Bidigare, R. R., Kennicutt, M. C., & Macko, S. A. (1995). Dependence of phytoplankton carbon isotopic composition on growth rate and $[CO_2]aq$: Theoretical considerations and experimental results. *Geochimica et Cosmochimica Acta*, *59*(6), 1131–1138. https://doi.org/10.1016/0016-7037(95)00030-4

Liu, H., Luo, L., & Cai, D. (2017). Stable carbon isotopic analysis of amino acids in a simplified food chain consisting of the green alga *Chlorella* spp., the calanoid copepod *Calanus sinicus*, and the Japanese anchovy (*Engraulis japonicus*). *Canadian Journal of Zoology*, *96*(1), 23–30. https://doi.org/10.1139/cjz-2016-0170

Longhurst, A. R., & Glen Harrison, W. (1989). The biological pump: Profiles of plankton production and consumption in the upper ocean. *Progress in Oceanography*, *22*(1), 47–123. https://doi.org/10.1016/0079-6611(89)90010-4

Lynn, R. J., & Simpson, J. (1987). The California Current system: The seasonal variability of its physical characteristics. *Journal of Geophysical Research*, *92*(C12), 12947–12966. https://doi.org/10.1029/jc092ic12p12947

Mantua, N. J., Hare, S. R., Zhang, Y., Wallace, J. M., & Francis, R. C. (1997). A Pacific interdecadal climate oscillation with impacts on salmon production. *Bulletin of the American Meteorological Society*, *78*(6), 1069–1079. https://doi.org/10.1175/1520-0477(1997)078%3C1069:apicow%3E2.0.co;2

Mantua, N. J., & Hare, S. R. (2002). The Pacific Decadal Oscillation. *Journal of Oceanography*, *58*(1), 35–44. https://doi.org/10.1023/a:1015820616384

Marañón, E., Cermeño, P., Latasa, M., & Tadonléké, R. D. (2012). Temperature, resources, and phytoplankton size structure in the ocean. *Limnology and Oceanography*, *57*(5), 1266–1278. https://doi.org/10.4319/lo.2012.57.5.1266

Masotti, I., Moulin, C., Alvain, S., Bopp, L., Tagliabue, A., & Antoine, D. (2011). Large-scale shifts in phytoplankton groups in the Equatorial Pacific during ENSO cycles. *Biogeosciences*, *8*(3), 539–550. https://doi.org/10.5194/bg-8-539-2011

Matthews, C. J. D., Smith, E. A. E., & Ferguson, S. H. (2024). Comparison of $\delta^{13}C$ and $\delta^{15}N$ of ecologically relevant amino acids among beluga whale tissues. *Scientific Reports*, *14*(11146), 1-9. https://doi.org/10.1038/s41598-024-59307-w

McCabe, R. M., Hickey, B. M., Kudela, R. M., Lefebvre, K. A., Adams, N. G., Bill, B. D., Gulland, F. M. D., Thomson, R. E., Cochlan, W. P., & Trainer, V. L. (2016). An unprecedented coastwide toxic algal bloom linked to anomalous ocean conditions. *Geophysical Research Letters*, *43*(19), 10,366-10,376. https://doi.org/10.1002/2016gl070023

McClatchie, S. (2014). *Regional Fisheries Oceanography of the California Current System*. Springer Dordrecht. https://doi.org/10.1007/978-94-007-7223-6

McClelland, J. W., & Montoya, J. P. (2002). Trophic relationships and the nitrogen isotopic composition of amino acids in plankton. *Ecology, 83*(8), 2173–2180. https://doi.org/10.2307/3072049

McGowan, J. A., Cayan, D. R., & Dorman, L. M. (1998). Climate-Ocean variability and ecosystem response in the Northeast Pacific. *Science*, *281*(5374), 210–217. https://doi.org/10.1126/science.281.5374.210

McGowan, J. E., Bograd, S. J., Lynn, R. J., & Miller, A. (2003). The biological response to the 1977 regime shift in the California Current. *Deep Sea Research Part II: Topical Studies in Oceanography*, *50*(14-16), 2567–2582. https://doi.org/10.1016/s0967-0645(03)00135-8

McMahon, K. W., Fogel, M. L., Elsdon, T. S., & Thorrold, S. R. (2010). Carbon isotope fractionation of amino acids in fish muscle reflects biosynthesis and isotopic routing from dietary protein. *Journal of Animal Ecology, 79*(5), 1132–1141. https://doi.org/10.1111/j.1365-2656.2010.01722.x

McMahon, K. W., Polito, M. J., Abel, S., McCarthy, M. D., & Thorrold, S. R. (2015a). Carbon and nitrogen isotope fractionation of amino acids in an avian marine predator, the gentoo penguin (Pygoscelis papua). *Ecology and Evolution*, *5*(6), 1278–1290. https://doi.org/10.1002/ece3.1437

McMahon, K. W., Thorrold, S. R., Elsdon, T. S., & McCarthy, M. D. (2015b). Trophic discrimination of nitrogen stable isotopes in amino acids varies with diet quality in a marine fish. *Limnology and Oceanography*, *60*(3), 1076–1087. https://doi.org/10.1002/lno.10081

McMahon, K. W., & McCarthy, M. D. (2016). Embracing variability in amino acid $\delta^{15}N$ fractionation: mechanisms, implications, and applications for trophic ecology. *Ecosphere*, *7*(12), 1-26. https://doi.org/10.1002/ecs2.1511

Newsome, S. D., Clementz, M. T., & Koch, P. L. (2010). Using stable isotope biogeochemistry to study marine mammal ecology. *Marine Mammal Science*, *26*(3), 509–572. https://doi.org/10.1111/j.1748-7692.2009.00354.x

O'Connell, T. C. (2017). "Trophic" and "source" amino acids in trophic estimation: a likely metabolic explanation. *Oecologia*, *184*(2), 317–326. https://doi.org/10.1007/s00442-017-3881-9

Ohkouchi, N., Ogawa, N. O., Chikaraishi, Y., Tanaka, H., & Wada, E. (2015). Biochemical and physiological bases for the use of carbon and nitrogen isotopes in environmental and ecological studies. *Progress in Earth and Planetary Science*, *2*(1), 1-17. https://doi.org/10.1186/s40645-015-0032-y

Ohman, M. D., Rau, G. H., & Hull, P. M. (2012). Multi-decadal variations in stable N isotopes of California Current zooplankton. *Deep Sea Research Part I Oceanographic Research Papers*, *60*, 46–55. https://doi.org/10.1016/j.dsr.2011.11.003

Oliver, E. C. J., Donat, M. G., Burrows, M. T., Moore, P. J., Smale, D. A., Alexander, L. V., Benthuysen, J. A., Feng, M., Sen Gupta, A., Hobday, A. J., Holbrook, N. J., Perkins-Kirkpatrick, S. E., Scannell, H. A., Straub, S. C., & Wernberg, T. (2018). Longer and more frequent marine heatwaves over the past century. *Nature Communications*, *9*(1324), 1-12. https://doi.org/10.1038/s41467-018-03732-9

Oliver, E. C. J., Benthuysen, J. A., Darmaraki, S., Donat, M. G., Hobday, A. J., Holbrook, N. J., Schlegel, R. W., & Sen, A. (2021). Marine Heatwaves. *Annual Review of Marine Science*, *13*(1), 313–342. https://doi.org/10.1146/annurev-marine-032720-095144

Palacios, D. M., Bograd, S. J., Mendelssohn, R., & Schwing, F. B. (2004). Long-term and seasonal trends in stratification in the California Current, 1950–1993. *Journal of Geophysical Research*, *109*(C10), 1-12. https://doi.org/10.1029/2004jc002380

Peterson, B. J., & Fry, B. (1987). Stable isotopes in ecosystem studies. *Annual Review of Ecology and Systematics*, *18*(1), 293–320. https://doi.org/10.1146/annurev.es.18.110187.001453

Peterson, W. T., & Schwing, F. B. (2003). A new climate regime in Northeast Pacific ecosystems. *Geophysical Research Letters*, *30*(17), 1-4. https://doi.org/10.1029/2003gl017528

Popp, B. N., Laws, E. R., Bidigare, R. R., Dore, J. C., Hanson, K. L., & Wakeham, S. G. (1998). Effect of phytoplankton cell geometry on carbon isotopic fractionation. *Geochimica et Cosmochimica Acta*, *62*(1), 69–77. https://doi.org/10.1016/s0016-7037(97)00333-5

Popp, B. N., Trull, T. W., Kenig, F., Wakeham, S. G., Rust, T. M., Bronte Tilbrook, F. Brian Griffiths, Wright, S. W., Marchant, H. J., Bidigare, R. R., & Laws, E. R. (1999). Controls on the carbon isotopic composition of southern ocean phytoplankton. *Global Biogeochemical Cycles,13*(4), 827–843. https://doi.org/10.1029/1999gb900041

Popp, B. N., Graham, B. S., Olson, R., Cecelia, Lott, M. J., López-Ibarra, G. A., Galván-Magaña, F., & Fry, B. (2007). Insight into the trophic ecology of yellowfin tuna, *Thunnus albacares*, from compound-specific nitrogen isotope analysis of proteinaceous amino acids. *Terrestrial Ecology*, *1*, 173–190. https://doi.org/10.1016/s1936-7961(07)01012-3

Post, D. M. (2002). Using stable isotopes to estimate trophic position: Models, methods, and assumptions. *Ecology*, *83*(3), 703-718. https://doi.org/10.1890/0012-9658(2002)083[0703:USITET]2.0.CO;2

Preti, A. (2020). *Trophic ecology of nine top predators in the California Current* [Doctoral dissertation, University of Aberdeen]. https://doi.org/10.13140/RG.2.2.20739.02085

Rau, G. H., Takahashi, T., & Marais, D. J. D. (1989). Latitudinal variations in plankton $\delta^{13}C$: implications for CO_2 and productivity in past oceans. *Nature*, *341*(6242), 516–518. https://doi.org/10.1038/341516a0

Rau, G. H., Sullivan, C. W., & Gordon, L. I. (1991). $\delta^{13}C$ and $\delta^{15}N$ variations in Weddell Sea particulate organic matter. *Marine Chemistry*, *35*(1-4), 355–369. https://doi.org/10.1016/s0304-4203(09)90028-7

Rau, G. H., Riebesell, U., & Wolf-Gladrow, D. (1996). A model of photosynthetic ^{13}C fractionation by marine phytoplankton based on diffusive molecular CO_2 uptake. *Marine Ecology Progress Series*, *133*, 275–285. https://doi.org/10.3354/meps133275

Rau, G. H., Riebesell, U., & Wolf-Gladrow, D. (1997). CO_{2aq}-dependent photosynthetic ^{13}C fractionation in the ocean: A model versus measurements. *Global Biogeochemical Cycles*, *11*(2), 267–278. https://doi.org/10.1029/97gb00328

Raven, J. A., & Johnston, A. M. (1991). Mechanisms of inorganic-carbon acquisition in marine phytoplankton and their implications for the use of other resources. *Limnology and Oceanography*, *36*(8), 1701–1714. https://doi.org/10.4319/lo.1991.36.8.1701

R Core Team. (2024). R: A language and environment for statistical computing (Version 4.4.0) [Software]. R Foundation for Statistical Computing. https://www.R-project.org/

Ruiz-Cooley, R. I., Koch, P. L., Fiedler, P. C., & McCarthy, M. D. (2014). Carbon and nitrogen isotopes from top predator amino acids reveal rapidly shifting ocean biochemistry in the outer California Current. *PLOS ONE*, *9*(10), 1-8. https://doi.org/10.1371/journal.pone.0110355

Ruiz-Cooley, R. I., Gerrodette, T., Fiedler, P. C., Chivers, S. J., Danil, K., & Ballance, L. T. (2017). Temporal variation in pelagic food chain length in response to environmental change. *Science Advances*, *3*(10), 1-8. https://doi.org/10.1126/sciadv.1701140

Ruiz-Cooley, R. I., Gerrodette, T., Chivers, S. J., & Danil, K. (2021). Cooperative feeding in common dolphins as suggested by ontogenetic patterns in $\delta^{15}N$ bulk and amino acids. *Journal of Animal Ecology*, *90*(6), 1583–1595. https://doi.org/10.1111/1365-2656.13478

Ruiz-Cooley, R. I., Anderson, C., Kudela, R., Dunkin, R., & Field, J. (2024). Perturbations in a pelagic food web during the NE Pacific large marine heatwave and persistent harmful diatom blooms. *Harmful Algae*, *140*, 1-13. https://doi.org/10.1016/j.hal.2024.102743

Sabadel, A. J. M., Van Oostende N., Ward, B., Woodward, M. S., Robert Van Hale, & Frew, R. (2019). Characterization of particulate organic matter cycling during a summer North Atlantic phytoplankton bloom using amino acid C and N stable isotopes. *Marine Chemistry*, *214*, 1-12. https://doi.org/10.1016/j.marchem.2019.103670

Sachs, J. P., Repeta, D. J., & Goericke, R. (1999). Nitrogen and carbon isotopic ratios of chlorophyll from marine phytoplankton. *Geochimica et Cosmochimica Acta*, *63*(9), 1431–1441. https://doi.org/10.1016/s0016-7037(99)00097-6

Schell, D. M. (2001). Carbon isotope ratio variations in Bering Sea biota: The role of anthropogenic carbon dioxide. *Limnology and Oceanography*, *46*(4), 999–1000. https://doi.org/10.4319/lo.2001.46.4.0999

Schlenger, A. J., Libralato, S., & Ballance, L. T. (2018). Temporal variability of primary production explains marine ecosystem structure and function. *Ecosystems*, *22*(2), 331–345. https://doi.org/10.1007/s10021-018-0272-y

Schmidt, K., Atkinson, A., Stübing, D., McClelland, J. W., Montoya, J. P., & Voss, M. (2003). Trophic relationships among Southern Ocean copepods and krill: Some uses and limitations of a stable isotope approach. *Limnology and Oceanography*, *48*(1), 277–289. https://doi.org/10.4319/lo.2003.48.1.0277

Smale, D. A., Wernberg, T., Oliver, E. C. J., Thomsen, M., Harvey, B. P., Straub, S. C., Burrows, M. T., Alexander, L. V., Benthuysen, J. A., Donat, M. G., Feng, M., Hobday, A. J., Holbrook, N. J., Perkins-Kirkpatrick, S. E., Scannell, H. A., Sen Gupta, A., Payne, B. L., & Moore, P. J. (2019). Marine heatwaves threaten global biodiversity and the provision of ecosystem services. *Nature Climate Change*, *9*(4), 306–312. https://doi.org/10.1038/s41558-019-0412-1

Smith, K. E., Burrows, M. T., Hobday, A. J., King, N. G., Moore, P. J., Sen Gupta, A., Thomsen, M. S., Wernberg, T., & Smale, D. A. (2022). Biological impacts of marine heatwaves. *Annual Review of Marine Science*, *15*(1), 119-145. https://doi.org/10.1146/annurev-marine-032122-121437

Sonnerup, R. E., Quay, P. D., McNichol, A. P., Bullister, J. L., Westby, T. A., & Anderson, H. L. (1999). Reconstructing the oceanic ^{13}C Suess Effect. *Global Biogeochemical Cycles*, *13*(4), 857–872. https://doi.org/10.1029/1999gb900027

Styring, A. K., Kuhl, A., Knowles, T. D. J., Fraser, R. A., Bogaard, A., & Evershed, R. P. (2012). Practical considerations in the determination of compound-specific amino acid $\delta^{15}N$ values in animal and plant tissues by gas chromatography-combustion-isotope ratio mass spectrometry, following derivatisation to theirN-acetylisopropyl esters. *Rapid Communications in Mass Spectrometry*, *26*(19), 2328–2334. https://doi.org/10.1002/rcm.6322

Tagliabue, A., & Bopp, L. (2008). Towards understanding global variability in ocean carbon-13. *Global Biogeochemical Cycles*, *22*(1), 1-13. https://doi.org/10.1029/2007gb003037

Takizawa, Y., Takano, Y., Choi, B., Dharampal, P. S., Steffan, S. A., Ogawa, N. O., Naohiko Ohkouchi, & Yoshito Chikaraishi. (2020). A new insight into isotopic fractionation associated with decarboxylation in organisms: implications for amino acid isotope approaches in biogeoscience. *Progress in Earth and Planetary Science*, *7*(50), 1-13. https://doi.org/10.1186/s40645-020-00364-w

Tieszen, L. L., Boutton, T. W., Tesdahl, K. G., & Slade, N. A. (1983). Fractionation and turnover of stable carbon isotopes in animal tissues: Implications for ^{13}C analysis of diet. *Oecologia*, *57*(1-2), 32–37. https://doi.org/10.1007/bf00379558

Venrick, E. L. (2002). Floral patterns in the California Current System off southern California: 1990-1996. *Journal of Marine Research*, *60*(1), 171–189. https://doi.org/10.1357/002224002762341294

Venrick, E. L. (2012). Phytoplankton in the California Current system off southern California: Changes in a changing environment. *Progress in Oceanography*, *104*, 46–58. https://doi.org/10.1016/j.pocean.2012.05.005

Volk, T., & Hoffert, M. I. (2013). Ocean Carbon Pumps: Analysis of Relative Strengths and Efficiencies in Ocean-Driven Atmospheric CO_2 Changes. *The Carbon Cycle and Atmospheric CO2: Natural Variations Archean to Present*, *32*, 99–110. https://doi.org/10.1029/gm032p0099

Walsh, R. G., He, S., & Yarnes, C. T. (2014). Compound-specific $\delta^{13}C$ and $\delta^{15}N$ analysis of amino acids: a rapid, chloroformate-based method for ecological studies. *Rapid Communications in Mass Spectrometry*, *28*(1), 96–108. https://doi.org/10.1002/rcm.6761

Ware, D. M. (1995). A century and a half of change in the climate of the NE Pacific. Fisheries Oceanography, *4*(4), 267–277. https://doi.org/10.1111/j.1365-2419.1995.tb00072.x

Wiley, A. A., Ostrom, P. H., Welch, A. J., Fleischer, R. C., Gandhi, H., Southon, J., Stafford, T. W., Penniman, J. F., Hu, D., Duvall, F., & James, H. F. (2013). Millennial-scale isotope records from a wide-ranging predator show evidence of recent human impact to oceanic food webs. *Proceedings of the National Academy of Sciences*, *110*(22), 8972–8977. https://doi.org/10.1073/pnas.1300213110

Wu, Y., Hain, M. P., Humphreys, M. P., Hartman, S., & Tyrrell, T. (2019). What drives the latitudinal gradient in open-ocean surface dissolved inorganic carbon concentration?. *Biogeosciences*, *16*(13), 2661–2681. https://doi.org/10.5194/bg-16-2661-2019

Yun, H. Y., Larsen, T., Choi, B., Won, E., & Shin, K. (2022). Amino acid nitrogen and carbon isotope data: Potential and implications for ecological studies. *Ecology and Evolution*, *12*(6), 1-22. https://doi.org/10.1002/ece3.8929

Appendix

Appendix A

Tables

Table 3. Stable isotope values of individual EAAs in skin samples of common dolphins (*Delphinus delphis*) from 1990 to 2008.

Year	Ile	SD Ile	Leu	SD leu	Lys	SD Lys	Met	SD Met	Phe	SD Phe	Val	SD Val	Thr	SDThr
1990	-19.4	0.52	-25.34	0.36	-13.52	0.59	-27.83	0.54	-25.27	0.77	-22.45	0.42	-8.10	0.69
1991	-17.64	0.54	-24.4	0.25	-11.98	0.32	-24.89	0.61	-25.06	0.6	-21.79	0.41	-5.74	0.64
1991	-17.89	0.19	-24.93	0.45	-13.36	0.47	-26.46	0.51	-26.08	0.12	-22.47	0.19	-6.41	0.25
1992	-18.37	0.26	-25.07	0.39	-13.21	0.29	-25.43	0.02	-26	0.1	-22.01	0.44	-6.74	1.18
1993	-17.55	0.35	-24.76	0.42	-13.16	0.44	-26.64	0.28	-25.04	0.09	-22.03	0.47	-5.17	0.61
1993	-17.3	0.24	-24.29	0.16	-11.66	0.06	-25.9	0.16	-24.87	0.3	-21.59	0.34	-5.17	0.00
1995	-17.28	0.85	-26.33	1.52	-17.82	2.03	-22.72	0.75	-25.17	0.77	-22.28	0.7	-5.10	1.99
1995	-15.48	0.51	-25.9	0.16	-16.53	0.04	-23.68	1.01	-24.21	0.7	-21.48	0.31	-3.61	1.00
1996	-17.44	1.38	-26.29	0.05	-17.74	1.28	-24.9	3.76	-25.5	0.29	-22.25	0.37	-9.54	3.48
1996	-15.53	1.3	-24.56	2.05	-14.93	2.12	-22.57	1.44	-24.66	0.82	-21.27	1.16	-3.22	0.18
1997	-17.47		-25.44		-16.31		-24.15		-25.69		-23.39		-4.11	
1997	-17.53	0.12	-25.26	0.44	-16.18	0.15	-25.12	0.48	-26.61	0.13	-21.86	0.25	-4.45	0.25
1998	-19.92		-24.94		-21.31		-26.18		-30.42		-21.75			
1998	-17.66	0.52	-23.73	0.31	-12.83	1.08	-25.24	0.58	-25.01	0.4	-20.84	0.04	-4.41	0.28
1999	-18.78	0.17	-23.8	0.14	-12.82	0.01	-27.1	0.79	-26.08	0.11	-21.43	0.22	-4.70	0.51
2000	-17.41	1.35	-23.64	0.46	-12.52	0.57	-25.62	0.33	-25.27	0.2	-22.28	0.07	-6.28	0.56
2000	-17.65	0.25	-23.51	0.11	-12.36	0.98	-26.27	1.15	-25.17	0.88	-21.65	0.95	-4.21	0.96
2001	-17.5	1.86	-23.2	0.66	-12.12	0.34	-26.04	0.2	-25.03	0.14	-21.04	0.42	-4.07	0.29
2002	-17.91	0.49	-22.39	0.62	-10.97	0.39	-25.53	0.32	-24.19	0.29	-20.64	0.1	-3.45	0.81
2002	-16.81	0.13	-22.84	0.5	-11.1	0.85	-25.14	0.36	-24.8	0.07	-21.73	0.52	-3.94	0.94
2003	-17.77	0.76	-23.25	0.74	-11.92	0.85	-25.56	0.15	-24.82	0.48	-21.93	0.28	-4.57	0.30
2003	-17.29	0.35	-23.28	0.21	-11.98	0.6	-26.3	0.57	-25.29	0.08	-22.72	0.05	-4.46	0.26
2004	-18.82	0.55	-25.86	0.41	-18.36	1.02	-26.61	0.74	-27.56	0.34	-22.9	0.39	-9.32	0.20
2005	-18.48	1.17	-25.36	1.7	-18.64	4.16	-26.05	2.11	-28.48	3.28	-21.91	0.89	-6.07	0.06
2005	-18.88	0.64	-24.05	0.98	-16.91	0.63	-28.93	0.38	-27.59	0.25	-21.54	0.74	-5.94	1.09
2006	-18.43	1.12	-23.82	1.11	-16.82	1.19	-27.84	0.19	-27.74	0.89	-21.36	0.87	-5.23	1.55
2007	-18.68	0.61	-24.71	1.35	-19.44	1.48	-27.24	0.9	-29.14	1.06	-23.06	1.49	-6.25	0.41
2008	-18.08	0.93	-23.13	1.43	-17.58	0.42	-27.6	0.06	-27.95	1.13	-21.15	0.18	-3.45	0.44
2008	-18.89	0.13	-23.78	0.61	-19.86	0.52	-27.88	0.09	-28.86	0.92	-22.46	0.21	-6.61	1.38

Abbreviations: Standard deviation (SD), Isoleucine (Ile), leucine (Leu), Lysine (Lys), methionine (Met), phenylalanine (Phe), valine (Val) and threonine (Thr).

Table 4. Descriptive statistics of bulk and amino acid carbon stable isotope values.

AA	Mean	Maximum value	Minimum value	Standard deviation	Variance	Range
Bulk	-18.331071	-17.08	-19.86	0.67504918	0.4556914	2.78
Ala	-15.479655	-13.81	-17.36	0.97217533	0.94512488	3.55
Asp	-15.257241	-12.65	-18.52	1.58568123	2.51438498	5.87
Glu	-8.4727586	-2.52	-13.7	3.53013547	12.4618564	11.18
Gly	-7.4427586	-3.1	-15.04	3.55788049	12.6585135	11.94
Pro	-14.592414	-13.57	-15.53	0.64773592	0.41956182	1.96
Ile	-17.856552	-15.48	-19.92	0.97017405	0.94123768	4.44
Leu	-24.408966	-22.39	-26.33	1.06423797	1.13260246	3.94
Lys	-14.963448	-10.97	-21.31	3.01697611	9.10214483	10.34
Met	-25.911034	-22.57	-28.93	1.48661011	2.21000961	6.36
Phe	-26.122759	-24.19	-30.42	1.63522366	2.6739564	6.23
Val	-21.905517	-20.64	-23.39	0.65661244	0.4311399	2.75
Thr	-5.368571	-3.22	-9.54	1.6455680	2.7078942	6.32

Abbreviations: amino acid (AA), alanine (Ala), aspartic acid (Asp), glutamic acid (Glu), glycine (Gly), and proline (Pro)Isoleucine (Ile), leucine (Leu), Lysine (Lys), methionine (Met), phenylalanine (Phe), valine (Val) and threonine (Thr).

Table 5. Summary of linear regressions of $\delta^{13}C$ of EAAs.

Amino Acid	Slope (Estimate)	Significance (p-value)	Adjusted R^2	Temporal Trend	Interpretation
Phe	-0.000455	0.002	0.277	Significant negative	Clear decrease over time.
Met	-0.000338	0.014	0.173	Significant negative	Moderate temporal decline.
Lys	-0.000604	0.033	0.126	Significant negative	Weak but significant negative trend.
Leu	+0.000237	0.017	0.164	Significant positive	Slight but significant increase over time.
Val	+0.000021	0.746	-0.033	Not significant	No temporal trend detected.
Thr	+0.000088	0.584	-0.026	Not significant	No temporal change detected.
Ile	-0.000132	0.157	0.038	Not significant	Non-significant negative trend.
EAA mean	-0.000163	0.198	0.026	Not significant	The average shows no clear trend, possibly due to cancellation.

Abbreviations: essential amino acid (EAA), isoleucine (Ile), leucine (Leu), lysine (Lys), methionine (Met), phenylalanine (Phe), valine (Val) and threonine (Thr).

Table 6. General Additive Models.

Model	Description
Model 1	AA ~ s(Time index)
Model 2	AA ~ s(Temp)
Model 3	AA ~ s(DIC)
Model 4	AA ~ s(CUTI)
Model 5	AA ~ s(Chl-a)
Model 6	AA ~ s(Temp) + s(DIC)
Model 7	AA ~ s(Temp) + s(DIC) + s(Chl-a)
Model 8	AA ~ s(Temp) + s(DIC) + s(CUTI)
Model 9	AA ~ s(Temp) + s(DIC) + s(Chl-a) + s(CUTI)
Model 10	AA ~ s(Time index) + s(Temp) + s(DIC) + s(Chl-a)
Model 11	AA ~ s(Time index) + s(Temp) + s(DIC) + s(Chl-a) + s(CUTI)
Model 12	AA ~ s(Time index) + s(Temp) + s(DIC)

Abbreviations: amino acid (AA), temperature (Temp), chlorophyll a (Chl-a), dissolved inorganic carbon (DIC), coastal upwelling transport index (CUTI).

Table 7. GAMs summary of individual amino acids.

Phenylalanine				**Lysine**			
Modelo	AIC	R^2	Deviance_exp	Modelo	AIC	R^2	Deviance_exp
Modelo_1	91.63115	0.60922264	0.69439475	Modelo_1	126.6231	0.61096164	0.68768772
Modelo_2	115.49483	-0.0260396	0.01060464	Modelo_2	150.6016	0.00534006	0.05964694
Modelo_3	111.83422	0.09563438	0.12793315	Modelo_3	150.5824	-0.010728	0.02536947
Modelo_4	113.69837	0.05322633	0.10683654	Modelo_4	149.4288	0.03505702	0.07665322
Modelo_5	116.36074	0.05763188	0.22512753	Modelo_5	150.8332	-0.0049679	0.04723123
Modelo_6	111.72055	0.13574028	0.20789635	Modelo_6	151.4881	0.00811381	0.10116715
Modelo_7	99.23934	0.52814799	0.69798228	Modelo_7	132.6929	0.56080684	0.71930048
Modelo_8	113.32348	0.1092236	0.2107638	Modelo_8	148.753	0.21012419	0.43701578
Modelo_9	101.35996	0.49737187	0.69338436	Modelo_9	104.0566	0.82389285	0.94335961
Modelo_10	65.78198	0.8526237	0.9358072	Modelo_10	105.7968	0.83024426	0.91521338
Modelo_11	47.98793	0.91000022	0.97358322	Modelo_11	105.4459	0.83114611	0.92278122
Modelo_12	101.35996	0.49737187	0.69338436	Modelo_12	102.962	0.84615088	0.92063194
Isoleucine				**Leucine**			
Model	AIC	R^2	Deviance_exp.	Model	AIC	R^2	Deviance_exp.
Modelo_1	75.00545	0.36313202	0.4852867	Modelo_1	65.70753	0.62500868	0.71044149
Modelo_2	83.03252	0.1506246	0.3001264	Modelo_2	90.79711	-0.0336561	0.00326023
Modelo_3	81.36715	0.10146643	0.1335569	Modelo_3	80.00109	0.38930195	0.5334653
Modelo_4	85.3868	-0.0321223	0.00473919	Modelo_4	89.79246	0.00732177	0.04924872
Modelo_5	85.52426	-0.0370264	1.02E-05	Modelo_5	90.74172	-0.0316838	0.00516201

Modelo_6	81.01261	0.22288717	0.3811602
Modelo_7	82.37556	0.12824809	0.226033
Modelo_8	83.75682	0.0839305	0.1844623
Modelo_9	83.36329	0.1838021	0.3912328
Modelo_10	78.08188	0.32806868	0.5134229
Modelo_11	75.67782	0.40786965	0.6287061
Modelo_12	76.75981	0.34670091	0.5071766

Modelo_6	80.98533	0.28570581	0.33672682
Modelo_7	81.85689	0.29483678	0.38199437
Modelo_8	78.42057	0.4421906	0.60956168
Modelo_9	56.75024	0.74172774	0.89524862
Modelo_10	60.58501	0.70590024	0.81087113
Modelo_11	60.61319	0.70928953	0.82419418
Modelo_12	49.14392	0.80631249	0.90603797

Methionine

Model	AIC	R^2	Deviance_exp.
Modelo_1	86.87636	0.59350264	0.67428796
Modelo_2	104.95975	0.22329269	0.35143088
Modelo_3	101.47643	0.26453223	0.32478393
Modelo_4	104.92686	0.13769291	0.16848959
Modelo_5	109.96623	-0.0259588	0.01068263
Modelo_6	102.12444	0.32342531	0.47453854
Modelo_7	100.69885	0.33224321	0.44626379
Modelo_8	100.09385	0.37626917	0.52680094
Modelo_9	96.3161	0.48160584	0.66234884
Modelo_10	69.50715	0.79840884	0.90854314
Modelo_11	81.62055	0.686521	0.7929342
Modelo_12	82.79627	0.6748246	0.7883398

Valine

Model	AIC	R^2	Deviance_exp.
Modelo_1	62.31007	-0.0008124	0.05283527
Modelo_2	62.82513	-0.0349898	0.00197408
Modelo_3	62.60724	-0.0272428	0.00944444
Modelo_4	62.34952	-0.0055122	0.04457329
Modelo_5	61.97388	0.00523273	0.05228509
Modelo_6	63.74604	-0.035539	0.03842805
Modelo_7	64.51603	-0.024051	0.09580023
Modelo_8	65.38238	-0.0627228	0.05214829
Modelo_9	66.04572	-0.0454761	0.12033399
Modelo_10	65.7126	-0.0458669	0.10354269
Modelo_11	66.49114	-0.0352851	0.16522742
Modelo_12	64.467	-0.0156865	0.11152326

Threonine

Model	AIC	R^2	Deviance_exp.
Modelo_1	112.2599	0.09968608	0.1636131
Modelo_2	114.9403	-0.018448	0.01792519
Modelo_3	115.4639	-0.0370018	3.39E-05
Modelo_4	114.972	-0.0050427	0.04713501
Modelo_5	115.4634	-0.0369842	5.09E-05
Modelo_6	116.2402	-0.0323908	0.04135138
Modelo_7	118.0894	-0.068119	0.04632231
Modelo_8	117.5316	-0.0477698	0.06449129
Modelo_9	119.4518	-0.0852903	0.07386235
Modelo_10	111.0504	0.24941846	0.4480719
Modelo_11	111.9775	0.23732736	0.461632
Modelo_12	115.708	0.04262475	0.1783874

*The shaded line indicates the model with the best fit.

Table 8. GAM summary of EAAs mean**.**

Term	edf	F	p-value	Interpretation
Time index	3.10	11.28	0.0003	Highly significant non-linear temporal variation. The relationship with time is not straight and may include curves such as peaks or troughs.
Temperature	6.02	3.72	0.0151	Complex and significant relationship (indicated by edf > 1).
DIC	3.35	4.77	0.0108	Non-linear relationship with DIC is also significant, but less complex.
Chl-*a*	1.00	7.96	0.0129	Linear relationship (edf ≈ 1) but significant. In this case, the GAM found that the best way to model this variable was with a straight line.

Abbreviations: general additive model (GAM), dissolved inorganic carbon (DIC), chlorophyll a (Chl-a),effective degrees of freedom (edf).

Figures

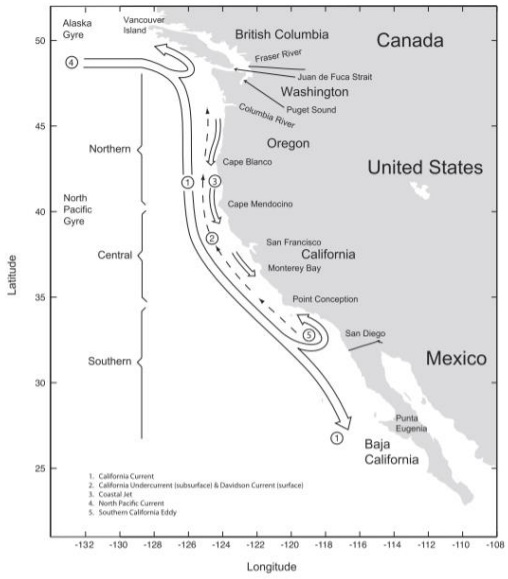

Figure 9. Map of the California Current System, taken from Checkley & Barth, 2009.

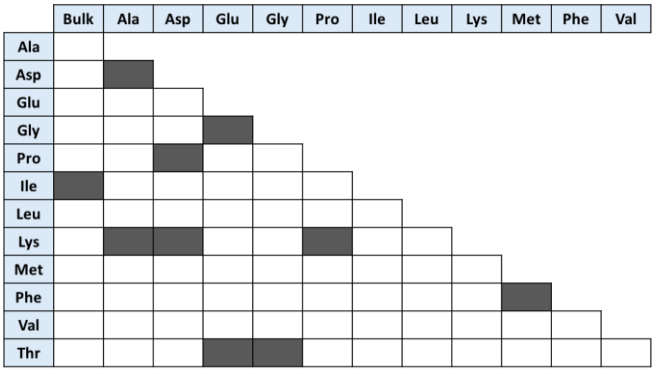

Figure 10. Pairwise comparisons between amino acids. Dark boxes indicate that there are no statistically significant differences (p-value > 0.05); empty boxes mean statistically significant differences (p<0.05).

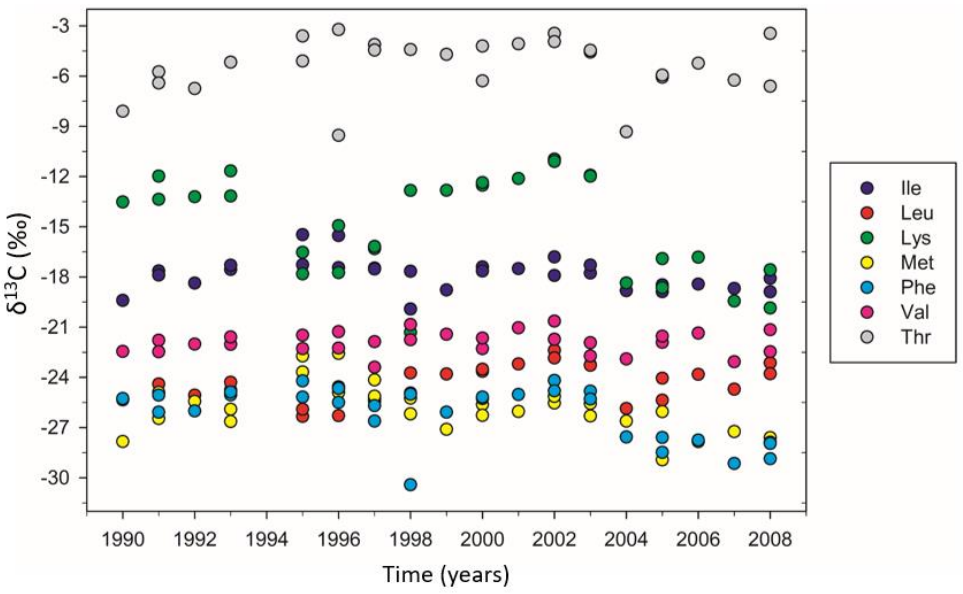

Figure 11. Time series of $\delta^{13}C$ values of EAAs of skin samples of common dolphins (*Delphinus delphis*) from 1990 to 2008. Isoleucine (Ile), leucine (Leu), lysine (Lys), methionine (Met), phenylalanine (Phe), valine (Val), and threonine (Thr).

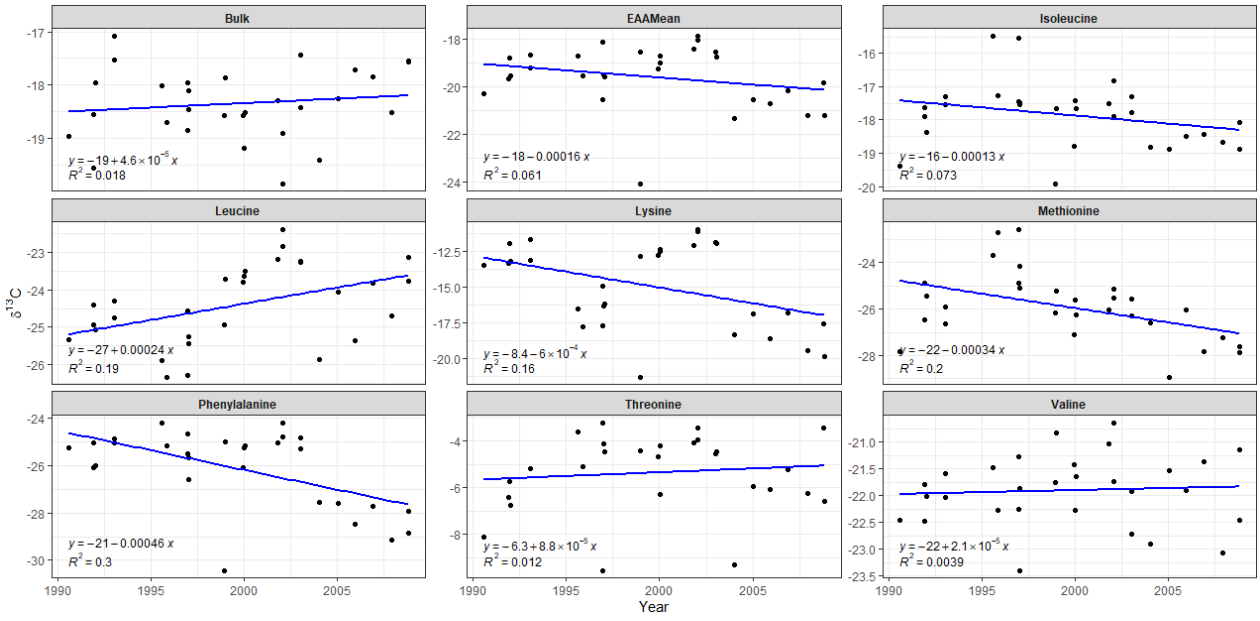

Figure 12. Linear regression of $\delta^{13}C$ values of EAAs.

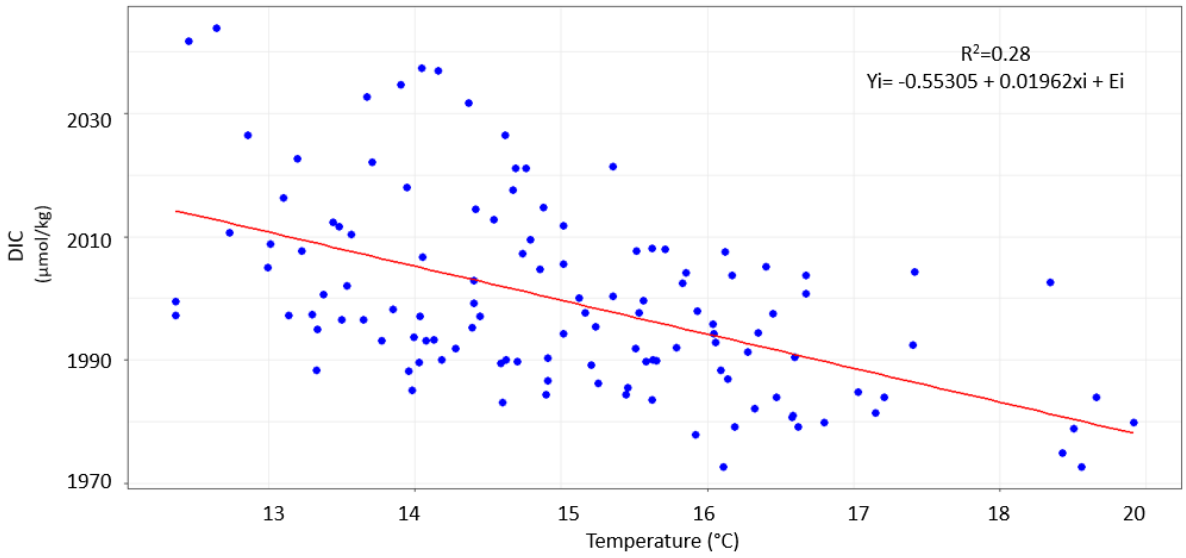

Figure 13. Linear regression of temperature and dissolved inorganic carbon.

At the 95% confidence level (alpha = 0.05) and with an R2 = 0.28, a moderate fit was concluded, as only 27.8% of the data explained the model: Yi = -0.55305 + 0.01962xi + Ei

Regarding the Pearson coefficient (R = 0.53), a moderate linear association can be described between the DIC variable (Y) and Temperature (X). Only 27.8% of the variability in DIC is explained by temperature. This indicates a significant, but not very strong, relationship. Water temperature has a negative and statistically significant effect on dissolved inorganic carbon (DIC) ($\beta = -5.51$, $p < 0.001$). However, the linear model explains only 27.8% of the observed variation in DIC, suggesting that other variables also influence its behavior.

Appendix B

Modeling Missing DIC Data

The study period for this project spans from 1990 to 2008; however, no dissolved inorganic carbon (DIC) data are available between 2002 and 2007. To supplement this information, a Bayesian multiple regression model was fitted based on water temperature (averaged from 0 to 50 m depth) and other predictors, including a linear time variable, a cyclical spline for monthly variability, and a first-order autoregressive term to capture temporal autocorrelation of the residuals.

Data

All available temperature and DIC data for our study area in the CalCOFI database (available at: https://calcofi.org/data/oceanographic-data/, accessed February 2025), spanning the period from 1983 to 2021, were used to increase the sample size and thus the accuracy of the estimates of missing DIC values. For temperature, the data are constant for this entire time series, with four values per year (one for each season). The average water temperature value from 0 to 50 m depth was calculated for each station sampled by the CalCOFI cruise (29 stations located within our study area). All station values were then summed to obtain an average value per cruise that is representative of the season.

In the case of DIC, information is available from 1983 to 2001 and from 2008 to 2021. DIC data from 1983 to 1993 are only available for line 90 (stations 90.70 and 90.90) and at a sampling depth of ~10 m. Since 2008, data from lines beyond line 90 were available in our study area and at several depths; however, only data from ~10 m depth and line 90 were considered to ensure consistency with the data from 1983 to 2001. In total, 176 temperature data points and 122 DIC data points were used to calibrate the model.

Predictors

The model was run using the brms package in R software version 4.4.0. Missing DIC data were modeled based on three components (equation 3):

1. **Water temperature** (linear predictor).

2. **Time index**: Captures linear trends over time.

3. **s(month)**: This is a cyclical spline (basis spline) that models monthly variation. If this value is close to zero, it means the model does not detect significant seasonality. If it is high, it indicates marked changes in DIC over the months of the year.

Formula: **DIC ~ Temperature + time index + s** (3)

and an autocorrelation structure: **AR[1]**

The first-order autoregressive (AR[1]) term captures the temporal autocorrelation in the residuals, which is particularly important in time series where consecutive observations are often correlated. This term is not part of the formula as a predictor but is incorporated into the model as a structural component. In the brms package, this term is applied not to the data themselves, but to the model residuals to capture their temporal dependence. First-order means that the value of the residual at time t depends on the residual at time t – 1 (equation 4). Its general formula is:

$$\varepsilon_t = \varphi_1 \cdot \varepsilon_{t-1} + \eta_t \quad (4)$$

Where:

εt: residual at time t
φ1: AR coefficient
ηt: random error

Results

The Bayesian model provided a good fit to the data, capturing both central tendencies and variability in the response. The results indicate that the model has a high predictive capacity, with an R^2=0.75 (95% CI: 0.71, 0.78). Four Markov chains were used, each with 10, 000 iterations (5,000 warm-up and 5,000 sampling iterations), for a total of 10,000 subsequent samples.

Model diagnostics confirmed adequate convergence of the chains ($\hat{R} \approx 1.00$) and sufficient effective sample sizes (ESS>1000). A Student distribution was used due to evidence of outliers. The posterior distribution of the parameter v (degrees of freedom) was estimated at 10.06 (95% CI = 2.80, 32.19), suggesting the presence of heavy tails in the residuals. This indicates that the data tend to include extreme values, making the Student-t distribution more appropriate and robust than the normal alternative.

Posterior predictive checks

The histogram (Figure 14) of the residuals shows an approximately symmetric distribution centered on zero, with no evidence of marked bias. Although heavy tails were observed in the data, suggesting the presence of extreme values, the use of a Student distribution for the model family adequately captured

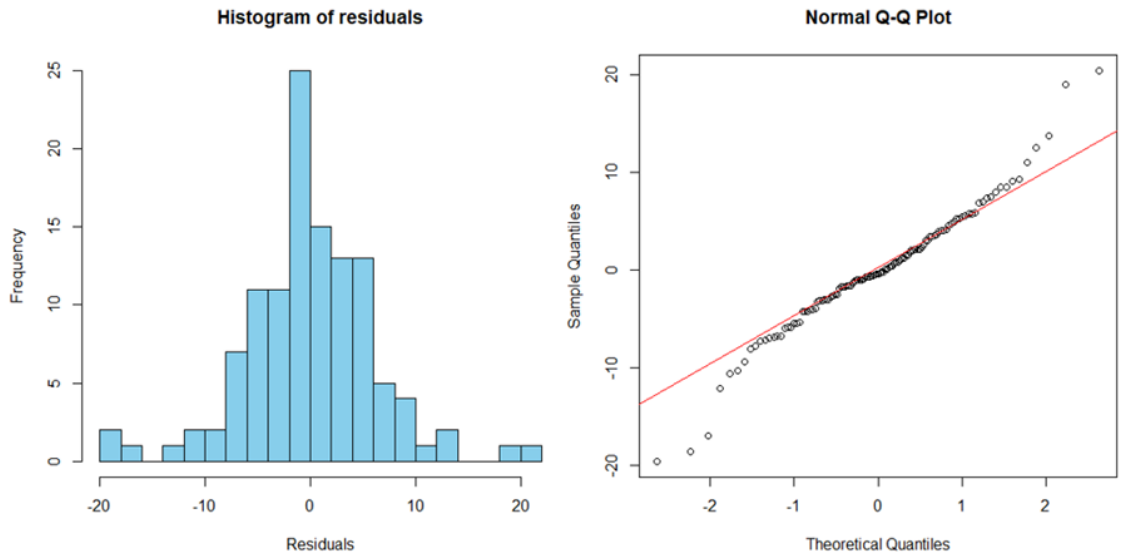

Figure 14. QQ plot and histogram of residuals.

this characteristic. This is supported by the QQ (quantile-quantile) plot, where the residuals reasonably follow the line expected under the theoretical distribution, with only slight deviations at the extremes.

Taken together, these results suggest that the model fits the data structure well, including the variability in the extreme values.

The Average Scatter Plot (Figure 15) compares the observed mean of the response variable (y) with the simulated means based on the model's predictions (yrep). The graph visually shows that the model's predicted mean is consistent with the observed mean in the data.

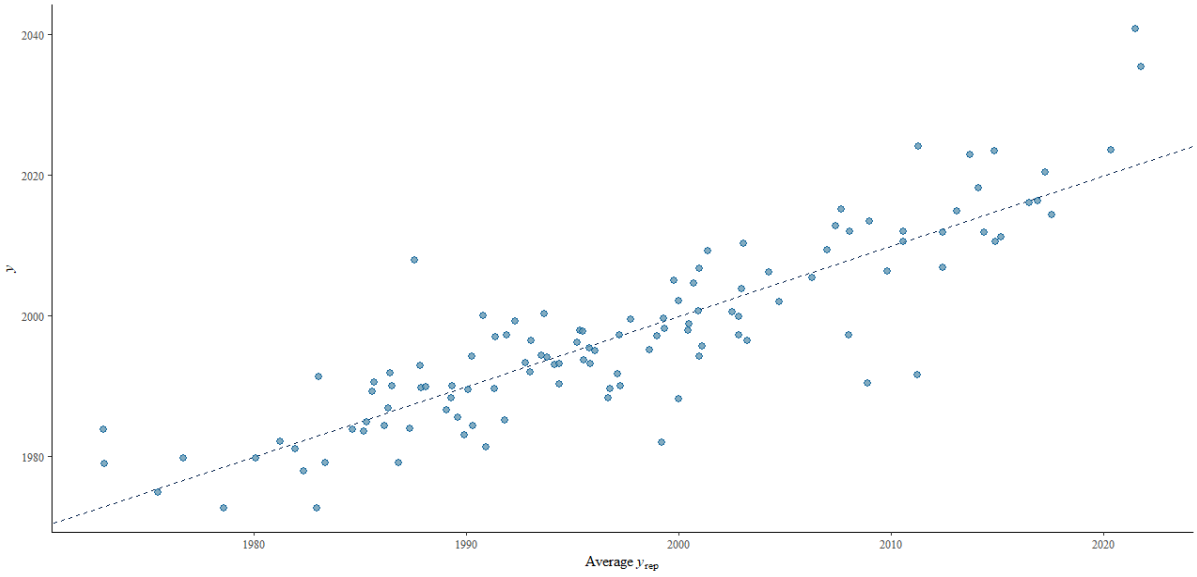

Figure 15. Average scatter plot. The dotted line is the observed mean of the actual data (mean(y)). The dots represent the means of the simulated predictions of each subsequent sample (mean (yrep[i,]) for each i).

The overlaid density plot compares the distribution of the simulated data (yrep) under the model with the actual data (y) (Figure 16). Because the posterior distributions (yrep) reasonably match that of y, the model has a good fit.

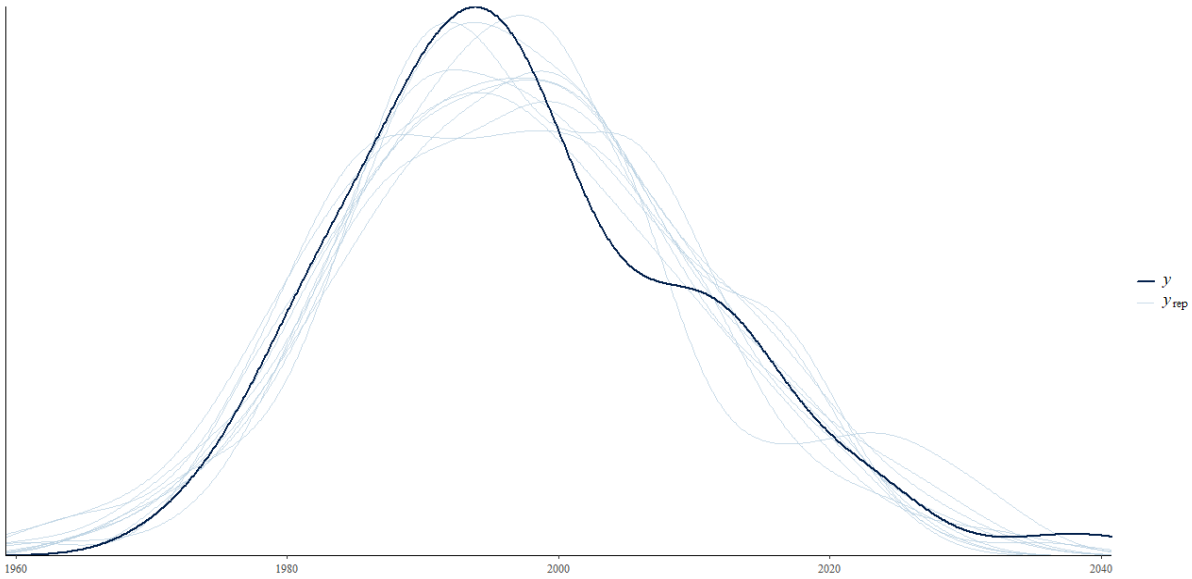

Figure 16. Overlaid density plot of the observed variable (y: black line) and model predictions (yrep: blue lines).

A credible negative effect of temperature on DIC was identified (estimate = −3.50; 95% CI: −4.74, −1.91), indicating that a 1°C increase in temperature is associated with an average decrease of 3.5 units in DIC. The time index presented a significant sustained positive effect (95% CI: 0.12, 0.21), suggesting an upward trend of 0.17 units in DIC per year throughout the study period. The monthly variability component (cyclical spline) showed moderate seasonal variation (estimate = 0.19, 95% CI: 0.07, 1.09) in DIC values throughout the year, i.e., DIC tends to vary with the month of the year, but this variation does not dominate the overall pattern. Temporal autocorrelation (AR) was moderate in magnitude, estimated at 0.51 (95% CI: 0.36, 0.58), meaning that there is moderate autocorrelation between the residuals from one month and those from the previous month, justifying its inclusion to improve the validity of the inferences. Overall, this model provided robust estimates of missing DIC values for the 2002–2007 period, considering the temporal structure and the relationship with available temperature data (Figure 17).

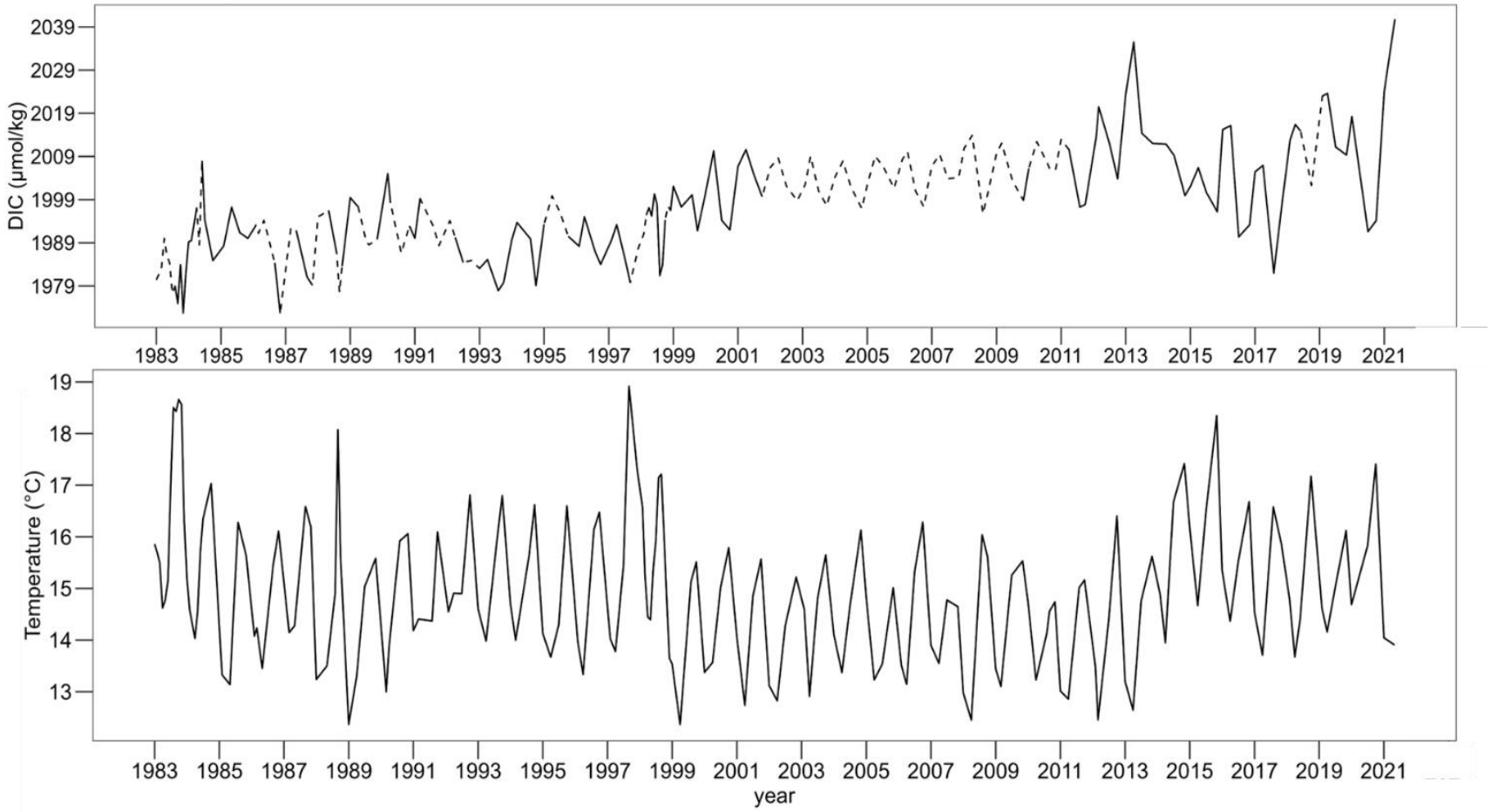

Figure 17. DIC and temperature time series from 1983 to 2021. In DIC the dotted line shows modeled values.